Analysis and Modeling of the Mechanical Durability of Proton Exchange Membranes Using Pressure-Loaded Blister Tests

Jacob R. Grohs

Thesis submitted to the faculty of the Virginia Polytechnic Institute and State University in partial fulfillment of the requirements for the degree of

Master of Science In

Engineering Mechanics

Dr. Scott W. Case - Committee Chairman

Dr. David A. Dillard

Dr. Michael W. Ellis

April 10th, 2009

Blacksburg, VA 24060

Keywords: proton exchange membrane, pressure-loaded blister test, digital image correlation, finite element analysis, lifetime prediction model

Analysis and Modeling of the Mechanical Durability of Proton Exchange Membranes Using Pressure-Loaded Blister Tests

Jacob R. Grohs

ABSTRACT

Environmental fluctuations in operating fuel cells impose significant biaxial stresses in the constrained proton exchange membranes (PEM). The PEM's ability to withstand cyclic environment-induced stresses plays an important role in membrane integrity and consequently, fuel cell durability. In this thesis, pressure loaded blister tests are used to study the mechanical durability of Gore-Select® series 57 over a range of times, temperatures, and loading histories. Ramped pressure tests are used with a linear viscoelastic analog to Hencky's classical solution for a pressurized circular membrane to estimate biaxial burst strength values. Biaxial strength master curves are constructed using traditional time-temperature superposition principle techniques and the associated temperature shift factors show good agreement when compared with shifts obtained from other modes of testing on the material. Investigating a more rigorous blister stress analysis becomes nontrivial due to the substantial deflections and thinning of the membrane. To further improve the analysis, the digital image correlation (DIC) technique is used to measure full-field displacements under ramped and constant pressure loading. The measured displacements are then used to validate the constitutive model and methods of the finite element analysis (FEA). With confidence in the FEA, stress histories of constant pressure tests are used to develop linear damage accumulation and residual strength based lifetime prediction models. Robust models, validated by successfully predicting fatigue failures, suggest the ability to predict failures under any given stress history whether mechanically or environmentally induced - a critical step in the effort to predict fuel cell failures caused by membrane mechanical failure.

ACKNOWLEDGEMENTS

I would like to thank my advisors Dr. Scott Case, Dr. David Dillard, and Dr. Mike Ellis who have encouraged and supported me since I began working with them as an undergraduate researcher in the Fall of 2005. More personally, I am touched by the effort of my committee to know me as a person of diverse interests and passions – they have supported me throughout my academic career in all of my pursuits, even those which would take me away from my research from time to time.

I would also like to thank General Motors, Corp and their financial support of my project over the past 3 years. In particular, interactions with Dr. Yeh-hung Lai and Gerald Fly have been particularly useful in furthering my research and my overall education.

I know that my experience here would never have been the same without the support and companionship of my lab-mates and fellow students on the GM project over the years. Thank you to Yongqiang Li, Kshitish Patankar, Edoardo Nicoli, Hitendra Singh, Michael Pestrak, Jessica Wright, and Chase Siuta. Best of luck in your future endeavors!

Finally, I owe much of my determination in finishing this degree to my wife, Courtney Grohs. Her loving support through the years has been paramount and she continues to astound me and make my life a happier and richer one. Thanks too, to my parents, Rich and Deb Grohs, for establishing an unconditional support system for me that has enabled me to take risks and live my life with purpose.

Table of Contents

List of Figures

List of Tables

Chapter 1: Introduction

Thesis Organization

This thesis is comprised of 3 separate manuscripts in various stages of preparation for submission to refereed scientific journals. Although the three works are valued as independent contributions, they represent a natural progression of the use of pressure-loaded blister tests in building a bridge from laboratory durability studies to the eventual goal of understanding material behavior within hydrogen fuel cell applications. The first article, found in Chapter 2 of this document, discusses the use of the blister test to study biaxial burst strength properties of PEM as a function of time and temperature. Building on the insight developed therein, the second article, Chapter 3, discusses using the Digital Image Correlation (DIC) method as well as finite element analysis (FEA) to investigate the appropriateness of utilizing uniaxially obtained constitutive models of the PEM in the large strain, biaxially loaded blister application. The third manuscript, presented in Chapter 4, extends the FEA work from Chapter 3 and uses published experimental data to develop lifetime prediction models capable of predicting observed failure times from blister testing.

Each manuscript, in the journey from data collection to eventual publication, represents the efforts of many coauthors; however, the author of this thesis is considered the major contributor and writer of each manuscript herein. Chapter 2 represents data collected, analyzed, and communicated by this author. Chapters 3 and 4 utilize data collected by co-authors, but all data analysis and written communication represent works by this author. In moving these drafts towards publication, this author is grateful for the significant co-author input - the honed manuscripts are truly a team effort.

Supplementary work lacking the impact or refinement for preparation in a formal journal article is found in the appendices. In particular, side studies are presented regarding the quantification of error induced by the DIC sphere fitting procedure described in Chapter 3 as well as the development of an alternative fitting program capable of digesting raw data from the DIC. Tabular summaries of relevant data and Mathematica® programs written to expedite calculations from within all manuscripts are also presented.

Motivation

Although experts continue to debate the social, economic, and environmental impacts of global energy use, it is clear that the transportation industry remains a critical player in the debate. In our country alone, transportation energy demands accounted for 67% of all liquid fuel use in the United States [1]. Debate aside, it is generally agreed that energy demand is ever increasing as our global energy needs evolve and, in particular, as developing countries progress. Scientists continue to argue over the reality/illusion of massive climate change due to our unrealistic energy demands. However, it is generally accepted that as humans, we are a contributor to widespread climate warming [2]. As discussed in [3], global dependence on fossil fuels (including liquid fuels such as petroleum used in the transportation industry) for our energy is not going to change in the short term. In this interim period, where fossil fuel reserves are still adequate for our energy demands, programs to develop alternative energies to meet global

needs have dramatically increased. One specific initiative of particular interest in the transportation industry is that of hydrogen powered fuel cell vehicles.

Hydrogen powered fuel cell vehicles have received both funding and interest, in large part, as an energy conversion system that could free the United States from the dependence on foreign oil. Hydrogen can be generated from a wide variety of sources, including non-carbon sources such as nuclear or solar power [4]. With economic and environmental forces driving further research, many consider hydrogen fuel cells to be one of the potential solutions to the current "global energy crisis." Although there are different types/methods of hydrogen powered fuel cells, the one of particular interest to this study is the proton exchange membrane fuel cell (PEMFC). PEMFC are commonly considered the most likely fuel cell candidate for the transportation industry because they exhibit high efficiencies as well as produce zero vehicular emissions [5].

In principle, PEMFC operation is simple. A thin sheet of PEM coated with a catalyst (usually platinum or platinum-carbon) layer is used to separate hydrogen fuel at the anode from oxygen in the air at the cathode [6]. When the hydrogen comes into contact with platinum catalyst, the hydrogen is split into its proton and electron constituents. The electrons travel through an external circuit, providing power, and meet with the protons which passed through the PEM. The protons and electrons then react with oxygen at the cathode to form water as a byproduct [7]. Although the electrochemical process is relatively simple and straightforward, many challenges face PEMFC as a competitive and reliable technology for transportation use. Some of these challenges, enumerated in [6], are: reliability and durability of the entire system, the ability to effectively and efficiently operate in the wide variety of environments vehicles are subjected to, reduction in costs of costly fuel cell components, and infrastructure for dispensing hydrogen as a fuel should vehicles be considered a replacement for current means of transportation. Thus the viability of PEM fuel cell vehicles is an interdisciplinary problem requiring technological, social, and economic changes. As such a complex problem, one intersection of Engineering Mechanics comes in studying and addressing the issue of fuel cell mechanical durability.

A recent review of PEM fuel cell durability literature outlined some of the potential mechanical failure modes of different PEMFC components leading to overall fuel cell failure. In particular, reference [8] studied the failures of the following key components: membrane, electrocatalyst and catalyst layer, gas diffusion layer, bipolar plate and the sealing gasket. Membrane degradation, which is of interest to this author, is further characterized in [8] as either caused by mechanical, thermal and/or chemical/electrochemical processes. Mechanical degradation of the PEM, the impetus for the works contained in this thesis, is thought to occur do to localized cracking or pinhole formation within the membrane which leads to reactant gas crossover and overall system failure. Mechanical degradation is often attributed to cyclic stresses introduced by the harsh and varied fuel cell operating environment. Not only are vehicles subject to a wide range of temperatures, but fuel cell operation typically requires temperatures around 90°C and humidity fluctuations from dry to completely hydrated. Much of recent literature has focused on modeling the effects of these environmental changes on the membrane and the corresponding induced biaxial stresses [9-12]. Although these works discuss biaxial loading, strength,

viscoelasticity, and modeling, it is done from a more holistic fuel cell assembly, or in-situ, approach. Early proof of concept work done by co-authors of the manuscripts presented in this thesis [13, 14], initiated a study of PEM mechanical durability ex-situ using pressure-loaded blister tests as a means of directly probing membrane strength and durability under biaxial loading. This thesis is the continuation and expansion of these initial studies in an effort to better understand and model membrane durability using fundamental mechanics of materials approaches.

Goals

From a big picture perspective, this work seeks to better understand fuel cell mechanical durability through investigation of membrane mechanical durability. As mentioned above, previous work [13] established the pressure loaded blister test as a means of studying membrane strength under biaxial loading conditions. In the extension and continuation of the proof of concept study, the following specific goals were outlined as critical steps in fully understanding membrane behavior within the blister test.

Characterize the biaxial burst strength of Gore-Select® Series 57 PEM (Chapter 2)

- Biaxial burst strength values are somewhat analogous to ultimate strength values calculated from uniaxial testing. By quickly ramping pressure until blister failure, the quasi-static membrane strength for different temperatures can be measured.
- Initial studies utilized rudimentary stress analysis methodology and assumed linear elastic material behavior. This characterization requires development of an appropriate linear viscoelastic solution.

Validate/Invalidate the use of the time temperature superposition principle (TTSP) to form biaxial burst strength master curves (Chapter 2)

- Collecting biaxial burst strength data for different time and temperature ranges will probe the success/failure of applying TTSP to the data set. Successful master curve generation would provide insight on a range of burst strength values for time/temperature.

Model the blister test using finite element analysis (FEA) to refine stress analysis (Chapter 3)

- FEA using linear viscoelastic constitutive data is a critical step in refining blister stress analysis tools since the FEA solution can capture localized true stresses within the membrane.
- Additionally, comparing the FEA solution with earlier methods serves to validate/invalidate those methods for use in further blister testing of PEM.

Validate the digital image correlation (DIC) methodology for use on blister studies of PEM (Chapter 3)

- The DIC is a powerful tool in experimental mechanics. However, the methodology requires spray painting the samples. The spray painted samples must be compared to

unpainted specimen and the effect of the spray paint on mechanical durability must be investigated.

Utilize the DIC technique in order to validate/invalidate the applicability of a small strain, uniaxial constitutive model to the blister geometry (Chapter 3)

- DIC blister stress analysis is independent of material properties. Comparison to constitutive based FEA results will validate/invalidate the application of small strain, uniaxially obtained linear viscoelastic properties for use in analyzing blister tests.

Develop a lifetime prediction model based on experimental data (Chapter 4)

- Using constant pressure blister data (somewhat analogous to traditional creep testing), linear damage accumulation (LDA) and residual strength based lifetime prediction models will be developed

Validate/Invalidate the lifetime prediction model in estimating lifetimes of more complex loading situations (Chapter 4)

- Since lifetime prediction models are calibrated on constant pressure testing, it is expected that they enjoy self-consistency in predicting other constant pressure test results. Validation/Invalidation of the model comes from making predictions on fatigue blister testing of PEM and comparing to experimental results.

Clearly, even a validated robust lifetime prediction model capable of predicting blister fatigue results does not directly translate to successful predictions of live fuel cell failure for given operating histories. However, it is the hope, that other ongoing research within Virginia Tech and other partners will eventually be able to accurately convert fuel cell vehicle fleet operating environments into equivalent applied membrane stress histories, which can then be run through the lifetime prediction models developed in this thesis. Since technology and knowledge continues to evolve, even as different membranes are studied, this thesis outlines a methodology which should enable future researchers to study and model the mechanical durability of tomorrow's fuel cell membrane materials.

In an effort to move towards the eventual goal of predicting fuel cell failures due to mechanical membrane failure, the manuscripts of this thesis discuss the use of the pressure-loaded blister test to study PEM durability characteristics as a function of time, temperature and load profile. Chapter 2 investigates biaxial burst strength properties; Chapter 3 utilizes DIC and FEA results to refine blister stress analysis procedures and validate the constitutive model; Chapter 4 extends the FEA work and uses published experimental data to develop lifetime prediction models for blister testing of PEM.

Chapter 2: Evaluating the Time and Temperature Dependent Biaxial Strength of Gore-Select® Series 57 Proton Exchange Membrane using a Pressure Loaded Blister Test

Abstract

Temperature and humidity fluctuations in operating fuel cells impose significant biaxial stresses in the constrained proton exchange membranes (PEM) of a fuel cell stack. The strength of the PEM, and its ability to withstand cyclic environment-induced stresses, plays an important role in membrane integrity and consequently, fuel cell durability. In this study, a pressure loaded blister test is used to characterize the biaxial strength of Gore-Select® series 57 over a range of times and temperatures. Hencky's classical solution for a pressurized circular membrane is used to estimate biaxial strength values from burst pressure measurements. A hereditary integral is employed to construct the linear viscoelastic analog to Hencky's linear elastic exact solution. Biaxial strength master curves are constructed using traditional time-temperature superposition principle techniques and the associated temperature shift factors show good agreement with shift factors obtained from constitutive (stress relaxation) and fracture (knife slit) tests of the material.

Introduction

Strength characterization of proton exchange membranes (PEMs) is critical for lifetime prediction of the membranes in fuel cell applications. The Department of Energy has set durability goals for PEM transportation applications at a 2000 hour service life by 2009 and a 5000 hour service life by 2013 [15]. These goals would hold PEM fuel cell vehicles to the same service life standards of today's current internal combustion engine systems. However, current fuel cell demonstration vehicles have yet to reach the DOE targets [16]. One reason is that under operating conditions and due to non-continuous usage, the fuel cell environment experiences both temperature and humidity fluctuations. When exposed to such hygrothermal changes, the membrane, which is clamped along the lands and seal gasket of fuel cells and constrained by the catalyst and gas diffusion layers, is expected to develop biaxial stress states. Lai et al. has shown that these imposed cyclic stresses can initiate crack formation, which leads to gas crossover and subsequent fuel cell failure [10]. In a previous work, Dillard et al. [13] showed that pressure loaded blister testing is a viable method to impose these biaxial stress states experimentally. In particular, pressure-ramped blister testing provides biaxial leakage or burst strength estimates which could be more descriptive of failure modes seen in working fuel cells than traditional strengths obtained by uniaxial tensile testing. Since biaxial burst strength values could provide insight into evaluating membrane durability, a means of experimentally and analytically obtaining these values while incorporating accurate material behavior is desired.

In early work with pressurized circular membrane testing, Hencky showed that stresses within the pressurized blister could be exactly determined for a linear elastic, homogeneous, isotropic membrane, using a power series solution [17]. The radial and tangential stresses, σ_r and σ_θ respectively, are given [17, 18] as:

$$\sigma_r(r) = \frac{1}{4}\left(\frac{Ep^2a^2}{h^2}\right)^{1/3} \cdot \sum_{k=0}^{\infty} B_{2k}\left(\frac{r}{a}\right)^{2k}$$
$$\sigma_\theta(r) = \frac{1}{4}\left(\frac{Ep^2a^2}{h^2}\right)^{1/3} \cdot \sum_{k=0}^{\infty} (2k+1)B_{2k}\left(\frac{r}{a}\right)^{2k} \qquad (2.1)$$

where E is the elastic modulus of the material, p is the applied pressure, a is the free radius of the blister, h is the thickness of the blister, and B_{2k} are coefficients to be determined through application of boundary conditions. By assuming zero residual mechanical strain, a reasonable approximation of σ_r and σ_θ at the center of a pressurized PEM blister test is given by,

$$\sigma_r = \sigma_\theta = \frac{B_0}{4}\left(\frac{Ep^2a^2}{h^2}\right)^{1/3} \qquad (2.2)$$

where $B_0 \approx 1.777$ for an assumed Poisson's ratio value of $v = 0.4$. Since Hencky's solution assumes a linear elastic material, modifications are needed to address the viscoelastic nature of polymers like PEM. To accurately explore time and temperature dependence of biaxial strength, material behavior due to environmental conditions must also be considered.

The viscoelastic response of polymers such as PEMs exhibits a dependence on temperature, time, and humidity. Early work with polymers led to the introduction of the time-temperature superposition principle (TTSP), which allows for the transformation of data from one temperature to another via horizontal shifts on a logarithmic time axis [19]. Alternately, short term viscoelastic properties such as relaxation modulus collected at different times and temperatures can be superimposed into a master curve describing behavior at times both shorter and longer than experimentally accessible. However, as noted in [19], the simple TTSP is not applicable to all polymers. Relevant to this study, success has been demonstrated in applying TTSP to Gore-Select® series 57. Specifically, Patankar et al. [20] studied the effects of both temperature and humidity on Gore-Select® series 57 and presented an initial linear viscoelastic characterization in the form of a relaxation modulus master curve along with hygrothermal shift factors.

The behavior of these viscoelastic membranes as relevant to our study is illustrated in Figure 2-1, as a plot of the Prony series approximation of the relaxation modulus master curve obtained from stress relaxation tests conducted on the Gore-Select® series 57 membranes tested in a dynamic mechanical analyzer as presented in [20]. It is important to note that the data of Figure 2-1 was collected under dry conditions to best simulate the uncontrolled humidity of the high temperature blister tests conducted above and is not identical to the curve presented in [20]. The regions denoted on the plot show the modulus variations within the time and temperature ranges of interest to this study.

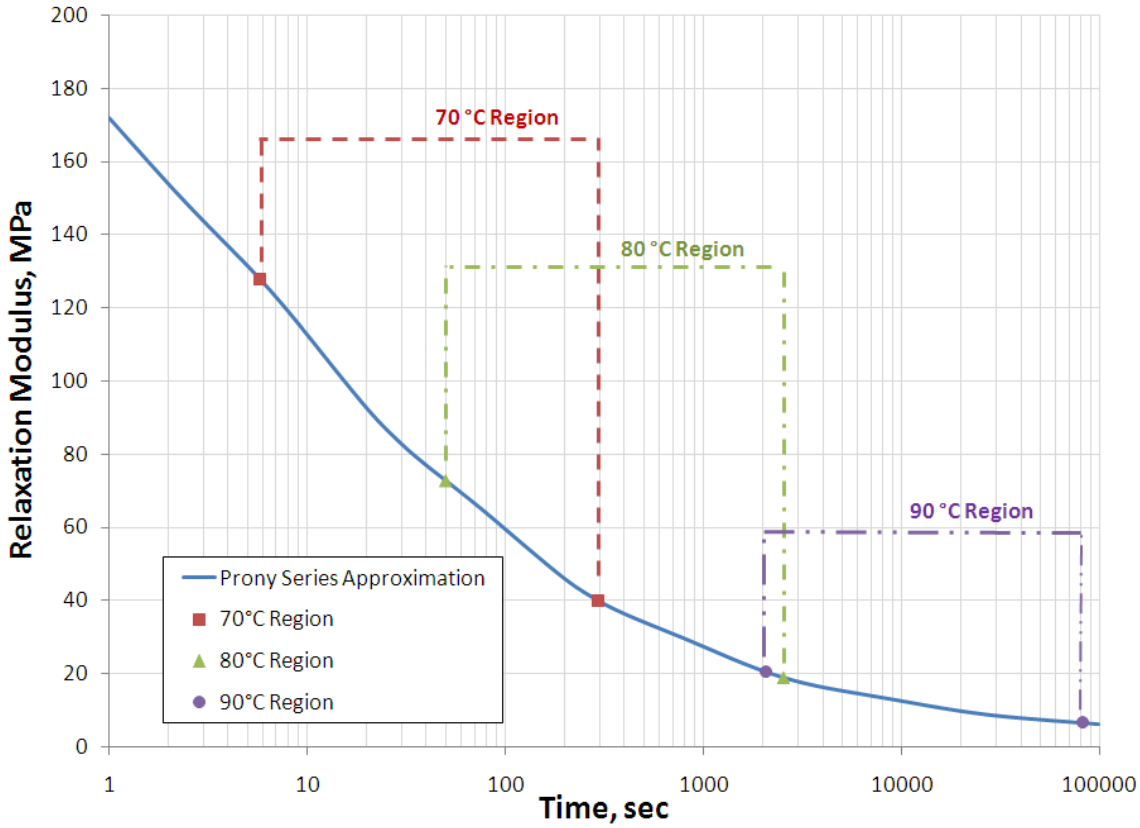

Figure 2-1: Plot of Prony series approximation of the relaxation modulus obtained from DMA tests of Gore-Select® series 57 under dry conditions with temperature regions denoted as applicable to the time range of the data utilized in this study.

It has been shown that the elastic-viscoelastic correspondence principle can be used to derive linear viscoelastic solutions from known linear elastic solutions provided the geometries and boundary conditions are identical [21]. Also known as Alfrey's correspondence principle, [22] describes the process of obtaining these linear viscoelastic solutions in detail. Each traction or displacement variable appearing in the analogous elastic solution is replaced by the Laplace transform of that variable. Next, any elastic constant appearing in the solution is replaced by the product of the Laplace variable *s* and the Laplace transform of the time dependent analog to the elastic constant. Having now obtained the linear viscoelastic solution in the Laplace domain, we then take the inverse transform to complete the procedure and provide the analogous, time dependent, linear viscoelastic solution. In application to Hencky's solution described above, the only variable requiring transformation into the Laplace domain is the applied pressure. Similarly, the only elastic constant appearing directly in Hencky's solution is the Young's modulus, *E*, whose corresponding time dependant viscoelastic property is the stress relaxation modulus *E(t)*. Although this principle is typically presented in traditional textbook examples, such as simple shaft torsion, this methodology has been shown broadly useful in solving more complex mechanics problems, such as in the indentation field [23, 24].

In applying the correspondence principle to Eq. (2.2) and taking the inverse Laplace transform, one obtains a hereditary integral formulation in which the stress relaxation modulus, *E(t)*, is

convoluted with the pressure input as the only other time dependant parameter. These modifications give σ_r and σ_θ at the center of a pressurized PEM blister as

$$\sigma_r(t) = \sigma_\theta(t) = \frac{B_0}{4} \cdot \left(\frac{a}{h}\right)^{2/3} \int_{-\infty}^{t} \left(E(t-\beta)\right)^{1/3} \cdot \frac{d\left[p^{2/3}(\beta)\right]}{d\beta} d\beta \qquad (2.3)$$

Building upon the above concepts, the objective of this study is to characterize the biaxial burst strength of Gore-Select® series 57 PEM over a range of time and temperature values using a pressurized blister test. A hereditary integral formulation of Hencky's classical solution will be employed using stress relaxation data obtained from the methodology in [20]. The TTSP will be independently applied to the collected data and the temperature shift factors obtained will be compared to the shift factors collected from constitutive (stress relaxation) and fracture (knife slitting) tests as described in [20, 25]. From application of TTSP, master curves will be generated that describe the effects of time and temperature on biaxial burst strength.

Experimental Procedure and Analysis

The pressurized blister testing method employed for PEMs in previous work [13] was expanded in this study to incorporate a range of test temperatures in order to investigate the applicability of the TTSP in pressure-loaded blister tests over temperatures relevant to operating fuel cells. Specifically, tests were conducted on Gore-Select® series 57 (Gore Fuel Cell Technology, Elkton, MD) at temperatures of 70°C, 80°C, and 90°C and readings of the pressure at burst and elapsed time at burst were collected. The experimental procedure, including sample preparation, heating to the desired test temperature, and pressurizing until bursting occurs, was described in detail in [13] and is only briefly reiterated here. Gore-Select® series 57 is an 18-μm-thick version of the perfluorosulfonic acid (PFSA) proton exchange membrane with a layer of micro-reinforced, composite expanded polytetrafluoroethylene (ePTFE). These micro-reinforced membranes have been shown to have improved tear resistance and dimensional stability compared to homogeneous cast membranes under some conditions [26, 27]. Gore-Select® series 57 membrane, as received, is sandwiched between two backings. One backing was removed before specimen preparation, while the other backing was retained throughout specimen fabrication to form consistent samples. Circular specimens were constructed using the front ferrules of standard Swagelok® tube fittings. A thin coat of Devcon® two-part five-minute epoxy was applied on the rim of the front ferrules, which were then inverted and placed onto a sheet of the membrane. After curing at room temperature, individual specimens were cut out using a razor blade, the second backing was removed, and the specimens were placed in a desiccator until specimen testing. To mount a specimen in preparation for testing, the front ferrule supporting a just taut membrane was placed into a Swagelok® ferrule nut and the assembly was screwed onto a Swagelok® reducing union. Once mounted on the pressure line, specimens were placed in an oven for environmental control and were pressurized using a KDScientifc® Series 230 syringe pump with atmospheric air as the working fluid. A schematic of the experimental setup is shown in Figure 2-2a and a photograph of the test in progress is shown in Figure 2-2b, respectively.

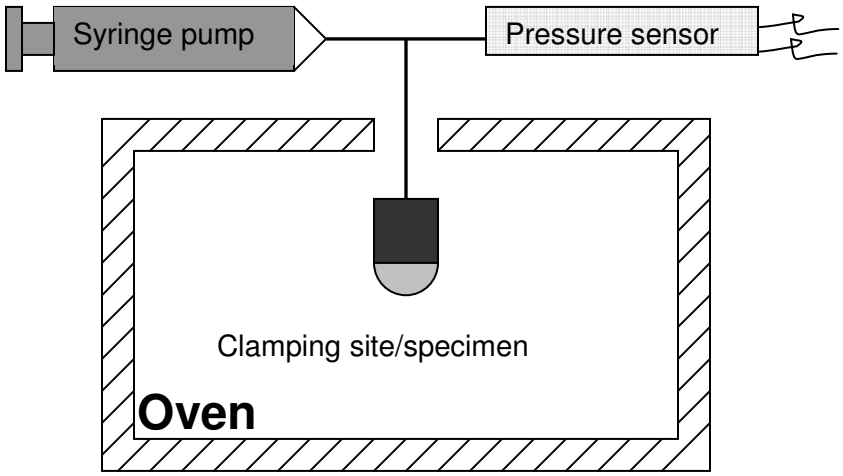

(a)

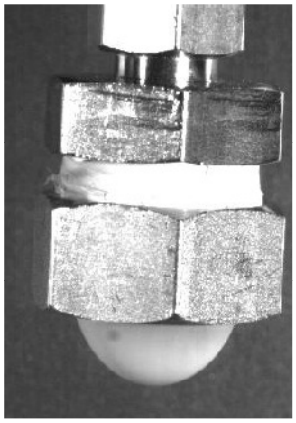

(c)

Figure 2-2: Illustrations of (a) experimental schematic diagram and (b) blister test in progress.

Raw pressure versus time data were collected from each test, where test initiation was marked by the first noticeable increase in pressure reading and bursting was denoted by catastrophic pressure loss. Successful testing of catastrophic burst failures was also verified in a qualitative way by the audible popping noise that accompanied such failures. Raw data from a selected representative sample is plotted as pressure versus time in Figure 2-3.

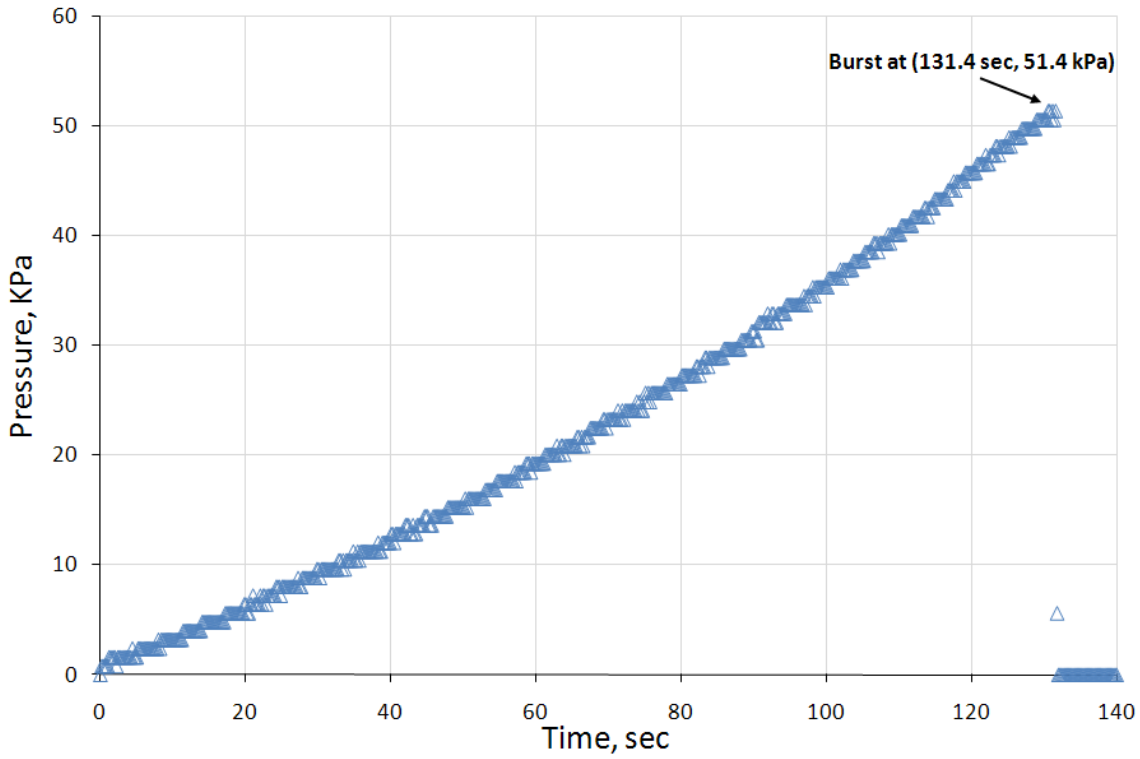

Figure 2-3: Raw pressure versus time data from representative sample of a Gore-Select® series 57 blister test conducted at 80℃ with a syringe pump infusion rate of 12 mL/min. Associated time and pressure at burst are illustrated.

From the collected readings from similar tests, burst pressures and times to failure were obtained for a series of syringe displacement rates and test temperatures. For the analysis of this data, Eq. (2.3) was utilized extensively using temperature appropriate relaxation modulus data given by the Prony series approximation for Gore-Select® series 57 presented in Figure 2-1. Although this approach proves to be a vast improvement over the assumptions of linear elastic behavior within the classical Hencky solution, it is imperative to objectively recall assumptions made in formulating this analogous linear viscoelastic solution. In the procedure, the relaxation modulus $E(t)$ was the only time dependent material property used in the modification and was convoluted in the integral with the applied pressure as a function of time, $p(t)$. Admittedly, the thickness will also be a time dependant parameter as the membrane continues thinning throughout the duration of the test. However, appropriate treatment of the thickness becomes quite complicated as it would involve not only applied stress levels at each instant in time but also a viscoelastic characterization of Poisson's ratio, $\nu(t)$, which is not well known or published for Gore-Select® series 57. To significantly reduce computational efforts, a constant value for the thickness of the membrane was assumed.

The motivation behind developing and employing this hereditary integral formulation was not just based on a desire to incorporate the time dependent relaxation modulus. The primary reason resulted from anomalous results found from an attempted application of TTSP to data obtained with an assumed constant elastic modulus. The results were temperature shift factors that were surprisingly large, approximately twice the values obtained from DMA testing. It was

known that as the hereditary integral formulation accounts for time dependency of the relaxation modulus, the overall slope of the biaxial burst strength versus time curve would become larger in magnitude compared to data with assumed constant elastic modulus. In application of TTSP, the steeper slopes of the hereditary integral method required less horizontal shifting to obtain overlap, thereby reducing the size of the temperature shift factors. This key concept of shift factor difference due to general slope difference is presented visually in Figure 2-4.

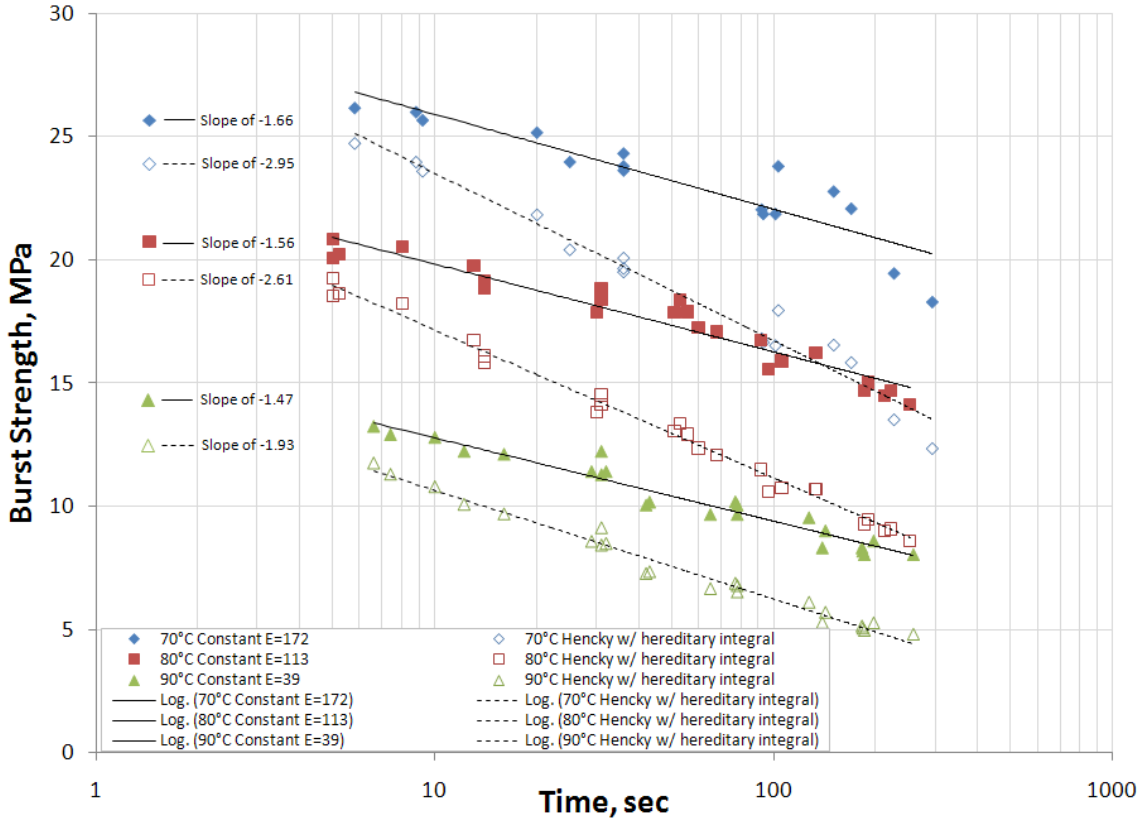

Figure 2-4: Comparison of slopes in curves obtained via constant elastic modulus and Hencky with hereditary integral methods.

The data reduction process outlined above provided a set of burst strength versus time to failure curves at selected temperatures. Traditional shifting methods were utilized to form a burst strength master curve with a reference temperature of 70°C. Temperature shift factors generated were then compared to shift factors obtained by stress relaxation and published knife slit tests in [25] under dry conditions to evaluate consistency.

Results and Discussion

Application of the hereditary integral to Hencky's solution led to a collection of burst strength values and associated times to failure over the temperature regions of interest. This data was then shifted using the traditional method of choosing a reference data set and sliding

subsequent data sets horizontally on a logarithmic time axis until visual alignment with the previous data set was obtained. No vertical shifts were employed. This method of visual shifting was used with a chosen reference temperature of 70°C to form the burst strength master curve featured in Figure 2-5.

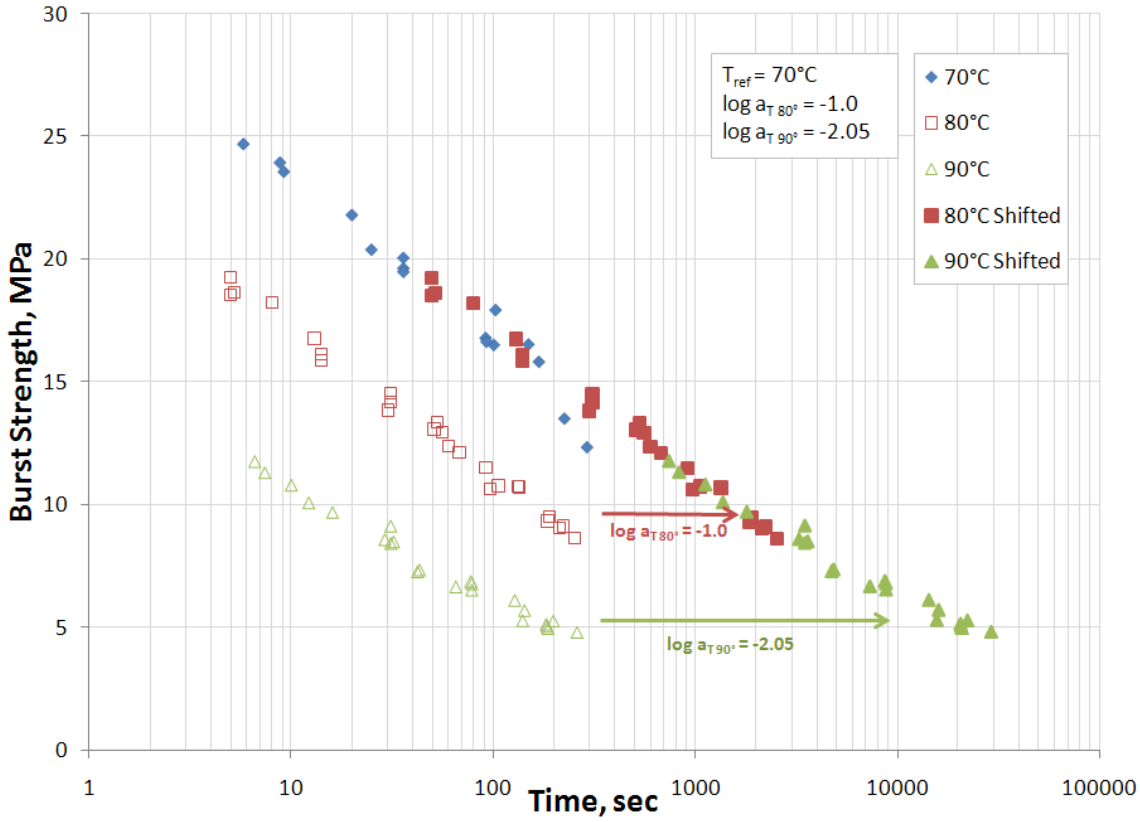

Figure 2-5: Burst strength data, calculated via Hencky's solution with a hereditary integral, shifted to form a master curve of Gore-Select® series 57 obtained using traditional shifting methods and referenced at 70°C.

As mentioned previously, the use of a hereditary integral with Hencky's solution gives an exact linear viscoelastic solution and is considered an improvement over the constant modulus approach. However, for completeness, a comparison plot of the burst strength master curves obtained via hereditary integral formulation of Hencky's solution and constant modulus approach is shown in Figure 2-6.

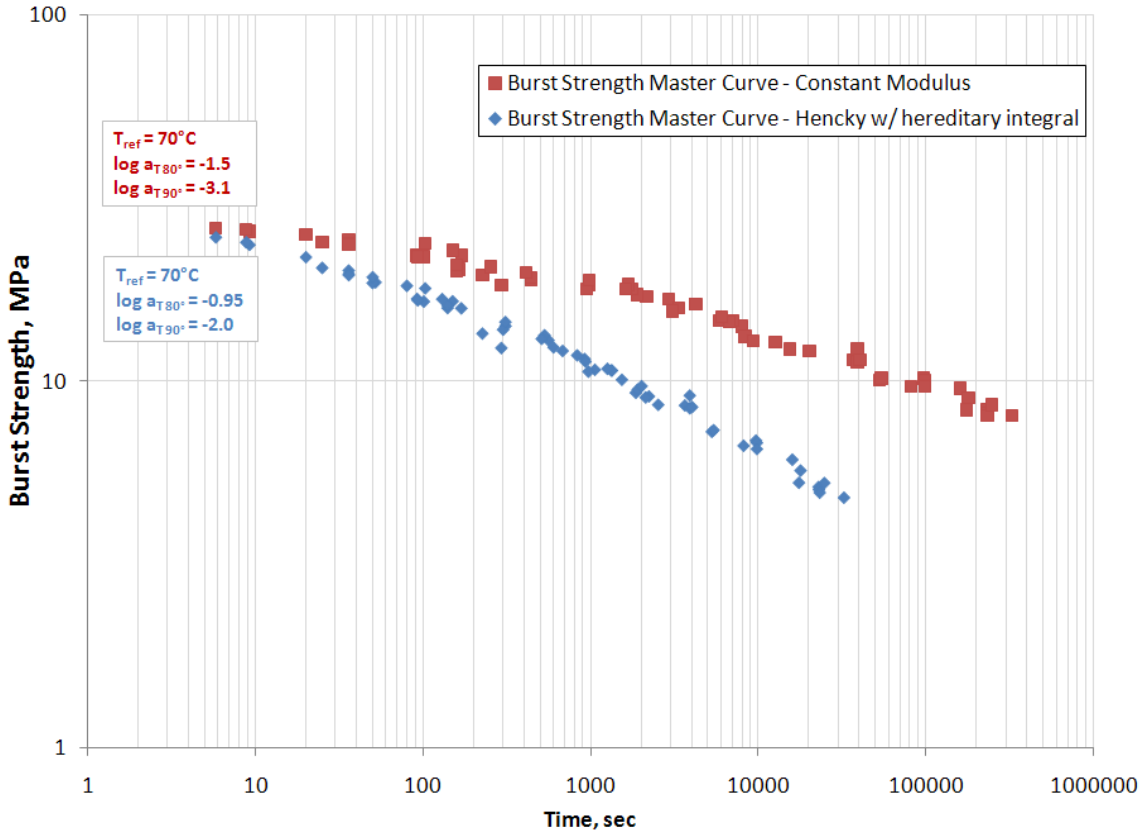

Figure 2-6: Comparison plot of burst strength master curves based on both Hencky's solution with a hereditary integral and constant modulus stress analysis methods.

One criterion for evaluating the appropriateness of TTSP is the consistency of shift factors obtained for different material properties [28]. It is therefore encouraging to note that in comparisons of these results with published shift factors obtained from stress relaxation tests and knife slitting tests, the Hencky solution with hereditary integral was found to be in reasonable agreement [20, 25]. This suggests that the same molecular relaxation processes that govern stress relaxation behavior and fracture in membranes also control the time dependent failures during biaxial loading. Figure 2-7 and Table 2-1 illustrate, in graphical and tabular forms, the agreement of the different temperature shift factors obtained for Gore-Select® series 57. Development of a burst strength master curve that provides shift factors comparable to those obtained from shifting constitutive data confirms the appropriateness of a viscoelastic framework for characterizing PEM behavior and suggests the possibility of basing lifetime prediction efforts on such accelerated tests. Although shift factor agreement does not guarantee success, it does support attempts to extend strength-life curve results from short time scales into longer lifetime investigations. This is the focus of an ongoing study.

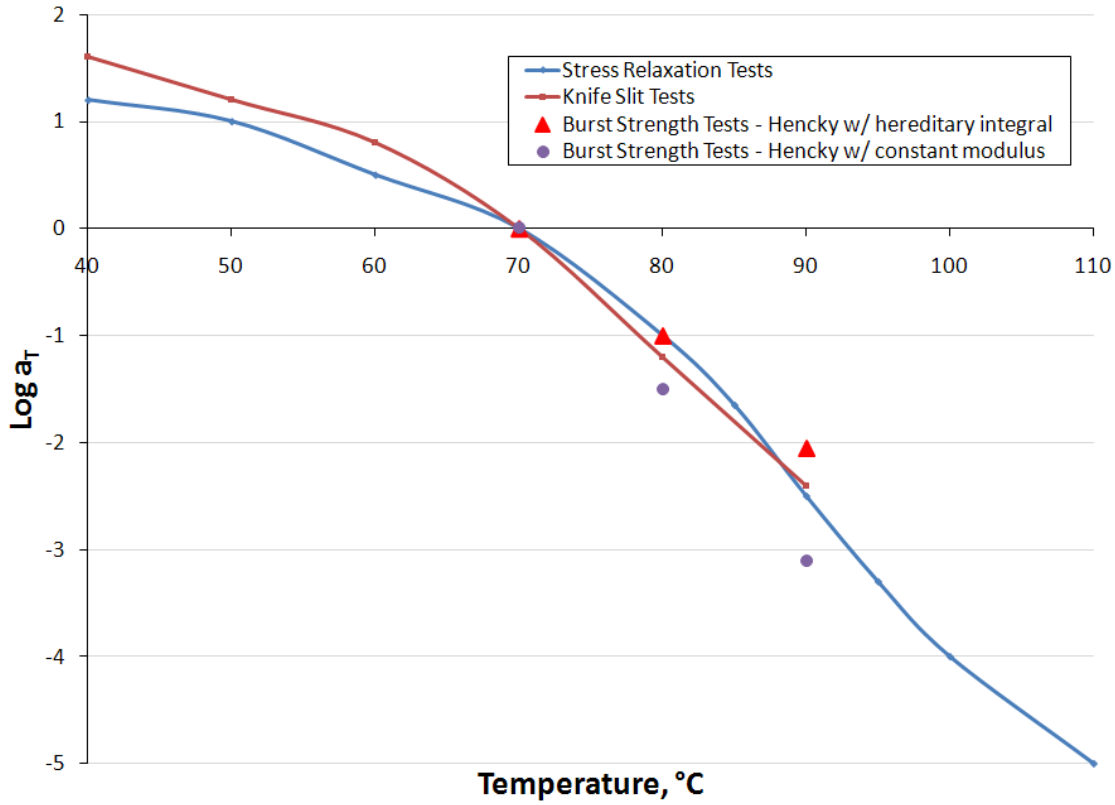

Figure 2-7: Plot of temperature shift factors obtained using methodology from [20, 25] for stress relaxation and knife slit tests and compared with shift factors obtained in this study.

Table 2-1: Biaxial strength shift factors for Gore-Select® series 57 from this study compared to those obtained with stress relaxation and knife slit tests [20, 25].

	70 °C	80 °C	90 °C
Stress Relaxation Tests	(reference)	-1.00	-2.50
Knife Slit Tests	(reference)	-1.20	-2.40
Burst Strength Tests – Hencky w/ hereditary integral	(reference)	-0.95	-2.00
Burst Strength Tests – Hencky w/ Constant Modulus	(reference)	-1.50	-3.10

Conclusions

Pressure loaded blister tests were used to characterize the biaxial strength of commercially available Gore-Select® series 57 membrane over a range of times to burst and temperatures of interest. The time temperature superposition principle was used to obtain biaxial strength

master curves using the traditional visual shifting method on data reduced via the Hencky solution with both a constant modulus and a hereditary integral linear viscoelastic solution; the resulting shift factors from the hereditary integral method were quite consistent with temperature shift factors obtained from stress relaxation and knife slitting tests.

While considering the encouraging insight and progress gained from this study, it is important to recall that the data reduction relies heavily on the linear viscoelastic material characterization from stress relaxation tests. This characterization, which provides no insight into nonlinear or elastic-plastic material properties, is still utilized in this study to treat a problem that likely involves both nonlinearity and plasticity. Although success was achieved via temperature shift factor agreement, the burst strength values presented are likely lower than the true values would be due to localized plasticity and the material nonlinearity. In spite of these approximations and omissions, the methodology is still useful as a cost and time effective tool in better understanding and improving PEM in operating fuel cells. In particular, these tests can be used to quickly screen membranes and compare the biaxial burst strength of one material to another. This data can also be used to investigate the critical issue of membrane durability and reliability. Repeated trials at identical loading rates can be used to begin statistical strength studies leading to material reliability constants based on an assumed statistical distribution. Additionally, a burst strength master curve under ramped pressure conditions can lend insight into possible relationships between applied stress levels and subsequent times to failure. Given a suggested relationship for time to failure as a function of applied stress, a damage evolution law can be applied and experimental failures under given loading conditions can be predicted. The ability to develop these techniques in such a simple and time-effective test would be invaluable if proven to predict more complex loading histories. If these efforts in lifetime prediction model are pursued and demonstrated with success, membrane durability could be investigated quickly and play a crucial role in achieving the DOE service life targets [29]. As another component to be added to this study, a similar characterization could be performed over a range of temperatures and relative humidities simultaneously to evaluate the hygrothermal dependence of the biaxial strength of Gore-Select® series 57. Finally, extending all of the applications mentioned into comparative studies of other commercially available membranes would provide valuable insight into behavioral differences among the products.

Acknowledgements

The authors are grateful to General Motors, Inc. for sponsoring and supporting this research and to the Department of Engineering Science and Mechanics and the Department of Mechanical Engineering at Virginia Tech for providing facilities and fostering interdisciplinary studies in fuel cell research. JRG also wishes to acknowledge the support of National Science Foundation Grant No. EEC-0552738.

Chapter 3: The Use of Digital Image Correlation and the Finite Element Method to Analyze Stresses in Pressure-Loaded Blister Tests of Proton Exchange Membranes

Abstract

Pressure-loaded blister tests have been used to characterize the biaxial burst strength of proton exchange membranes (PEMs). The stress analysis for these tests becomes nontrivial due to substantial center deflections and thinning of the PEMs. In this study, the digital image correlation (DIC) technique is used to measure full-field displacement and strain in the membrane under ramped pressure and constant pressure loading. Since the DIC method uses paint-speckled membranes, the effect of the speckling on mechanical durability is studied by comparing lifetime plots of both painted and unpainted specimen. It is concluded that the speckling method has no significant impact on the response for this application. The displacements obtained with the DIC are then used to validate the constitutive model and methods of the finite element analysis. With this coupled experimental and numerical stress analysis procedure, biaxial burst strength values calculated following the classical Hencky analysis reported in earlier studies are refined to supplement ongoing work in developing lifetime prediction models for fatigue failure of PEMs.

Introduction

Characterizing mechanical degradation of the proton exchange membrane (PEM) remains a critical issue in understanding failure of fuel cell systems. Although potential fuel cell failure modes can be any combination of mechanical, chemical, or electrical related issues, previous studies by Lai et al. in [10, 30] have shown that one mechanically induced failure mode is gas crossover due to crack formation. These cracks could develop due to imposed cyclic, biaxial stresses caused by hygrothermal fluctuations as the fuel cell routinely transitions between operating environments. In order to evaluate these biaxial stresses and the effect on membrane strength and durability, pressure-loaded blister tests have been studied. Early work by Dillard et al. introduced the concept of using these blister tests—which introduce a biaxial state of stress—as an improved and more representative study of membrane strength and durability relative to fuel cell applications than traditional uniaxial testing methodology [13]. Continuations of this work led to characterizations of the temperature dependence of biaxial burst strength, through the extension of Hencky's classical solution [17] for a pressurized circular linear elastic membrane into a linear viscoelastic solution, and the study of long term membrane durability via constant pressure (somewhat analogous to creep) and fatigue to leak blister testing [14, 31]. Although these studies have significantly advanced the understanding of membrane mechanical durability, all of the calculated strength values are dependent on the linear viscoelastic constitutive model of the membrane, as well as the assumptions required to apply the elastic-viscoelastic correspondence principle to Hencky's solution. The determination of the stresses based solely on the measured deformed geometry of the blister (as well as the known applied pressure) provides us with the capability to study the validity of the linear viscoelastic constitutive model. Successful demonstration of the applicability of such a constitutive model, developed based on small strain, uniaxial testing of PEM, into the large deflection, biaxially

loaded blister problem would suggest that material models of [20, 32] can be used in developing stress models to analyze the imposed stresses due to hygrothermal changes.

One advantage of the blister geometry is that the central portion of the blister experiences an equal biaxial stress state, which also represents the location of maximum stress [17, 18]. This state of equal biaxial stress in the blister can be modeled as a spherical cap in which the curvature of the thin film at the center of the blister is equal in all directions. Recalling fundamental mechanics relationships, the stresses within this spherical cap are analogous to those from thin wall spherical pressure vessel theory, in which the hoop stress, σ_θ, and radial stress, σ_r, are given in [33] as

$$\sigma_\theta = \sigma_r = \frac{pr}{2h} \qquad (3.1)$$

where *p* is the applied pressure, *r* is the radius of the sphere, and *h* is the thickness of the material. It is apparent that this spherical cap model of the central region of the blister geometry allows for determining the stresses independently of any material constitutive model. Because the applied pressure and membrane thickness are initially controlled and known quantities, the stresses can be calculated directly provided radius of curvature values can be obtained.

Since radius of curvature can be directly obtained by measuring the deformed shape of the blister, the digital image correlation (DIC) technique's ability to measure full-field 3-dimensional displacement data is of particular interest. The DIC methodology has been used with success in applications ranging from micro-scale strain concentrations in ductile fracture of Al 6061-T651, to adhesion experiments using a cylindrical blister test, to biaxial tension testing of textile weaves [34-36]. One necessary aspect of the DIC method is that the specimen surface have a random patterning that can be tracked during deformation in order to measure deformations. One of the most elementary methods of achieving a uniform random speckle pattern on the sample is lightly misting with commercial spray paint. In this study, the GOM Aramis 3D deformation measurement system is used to measure the membrane deformations and post-process the data.

To validate the linear viscoelastic constitutive model, two different means of material property dependent stress analysis methods are compared to the thin wall pressure vessel theory method proposed above. The first analysis method, as developed in [31], is the linear viscoelastic analog to Hencky's classical linear elastic solution where σ_r and σ_θ at the center of a pressurized PEM blister is given by

$$\sigma_r(t) = \sigma_\theta(t) = \frac{B_0}{4} \cdot \left(\frac{a}{h}\right)^{2/3} \int_{-\infty}^{t} \left(E(t-\beta)\right)^{1/3} \cdot \frac{d\left[p^{2/3}(\beta)\right]}{d\beta} d\beta \qquad (3.2)$$

where *E(t)* is the stress relaxation modulus of the material, *p* is the applied pressure, *a* is the free radius of the blister, *h* is the thickness of the blister, and B_0 is calculated to be 1.777 for an

assumed Poisson's ratio of ν=0.4. The second method of blister stress analysis is through an axisymmetric shell model defined with linear viscoelastic properties and subjected to a pressure load using the commercial finite element analysis (FEA) program ABAQUS.

The objective of this study is to use the DIC technique to measure the deformed shape of pressure-loaded blister tests on the commercially available Gore-Select® series 57 PEM in order to calculate imposed stresses independently of material constitutive model. Tests will be conducted at 90°C, a temperature within the operating range of current fuel cells, under ramped pressure and constant pressure loading conditions. To ensure that paint speckling used with the DIC method has no significant impact on the membrane's mechanical durability, the lifetimes of paint-speckled membranes will be compared to unpainted membranes. Once we have established confidence in the method, we will compare the stresses calculated from DIC deformation measurements to stress histories obtained via the linear viscoelastic analog to Hencky's solution as well as finite element models in ABAQUS. Agreement (as well as discrepancies) will validate/invalidate the use of a linear viscoelastic constitutive model to investigate imposed biaxial stresses due to temperature and humidity fluctuations within operating environments of PEM fuel cell applications.

Experimental Procedure and Analysis

The single ferrule system of pressure-loaded blister testing described in [13, 31] was improved and expanded in this study to incorporate more control over blister pressurization as well as integrating the DIC camera system to measure blister deformations. As specimen mounting and detailed procedures were presented in the earlier works, only the improvements will be discussed here. In past work, a syringe pump was used to introduce pressure into the blister; different volume infusion rates were found to roughly correspond to different linear ramp rates for the pressure. To improve resolution on ramped pressure testing, and to enable the testing of membrane samples under constant pressure (somewhat analogous to creep testing), a compressed air tank controlled by an electro-pneumatic pressure regulator was implemented, replacing the syringe pump used in previous work. DIC measurements were made by capturing images of through a single pane viewing glass in the oven used to control the blister environment. This imaging through glass method was employed so that the cameras would have proper perspective as the blister grows towards the cameras. Prior to mounting the specimen for testing, Krylon® black spray paint was used to lightly mist the specimen to provide the random speckle pattern needed by the DIC. Although consistency is more difficult to maintain in the application of random patterns, care was taken to provide nearly uniform coverage from specimen to specimen. Additionally, before testing each individual specimen, the DIC software was used to evaluate the quality of the initial speckle pattern. If the software was unable to define all points on the blister, as was the case for specimens in which the coverage was too heavy or too light, the sample was not used for testing. An image of the test setup with DIC cameras imaging through the oven can be seen in Figure 3-1 (a) while a mounted paint-speckled specimen is shown in Figure 3-1 (b).

(a)

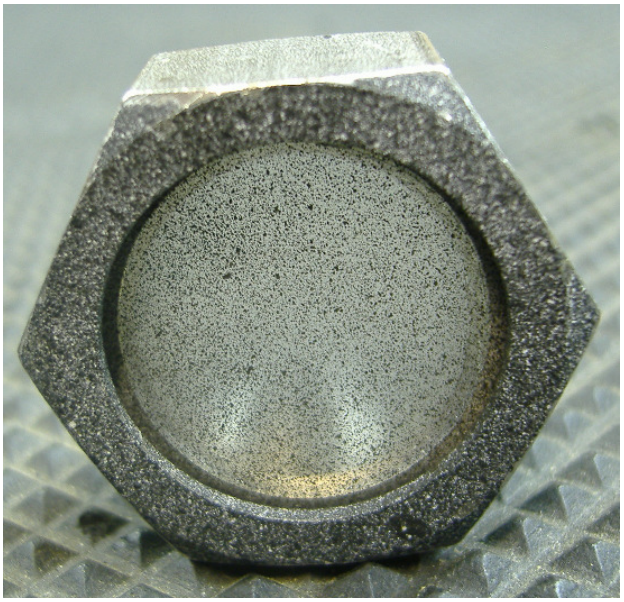

(b)

Figure 3-1: Images of (a) blister test setup with DIC cameras and (b) mounted paint-speckled specimen

In addition to the software screening process, the effects on mechanical durability due to painting the membrane as well as variability in the painting procedure is an important investigation within this study. Specifically, both painted and unpainted samples of Gore-Select® series 57 membrane were tested under both ramped pressure and constant pressure loading at 90°C. As in earlier work, the applied pressure was recorded throughout the test until after membrane rupture. For all painted samples, Schneider-Kreuznach cameras with 50 mm lenses were used to capture images periodically throughout the test. The camera sampling rate was adjusted between 0.1 frames per second (fps) and 1 fps in order to maximize the number of pictures taken during each test while remaining within the limitations of the software to store a finite number in memory. Specifically, a 25 x 25 mm field of view was used on all imaging. Aramis conservatively reports the overall accuracy of the system to be 1/30,000th of the field of view for out-of-plane measurements.

Once all of the images were taken, the undeformed blister geometry was calculated on the basis of two initial reference images taken immediately before pressurization began. Two images are used so that any measurement difference within the two nominally identical frames provides a quantitative measure of the scatter within the measurement for each specimen. Images are then solved frame by frame using a facet size of 13 and a step size of 11. Facet size is a measurement of the size of each element used in approximating the blister while the step size is a measure of the distance from the left edge of one facet to the left edge of the adjacent facet. In choosing a step size less than the facet size, facet overlap is ensured. These sizes are chosen to maximize the amount of data obtained per sample without compromising measurement resolution. A DIC image of the blister with the selected facet size overlaid for perspective is shown in Figure 3-2.

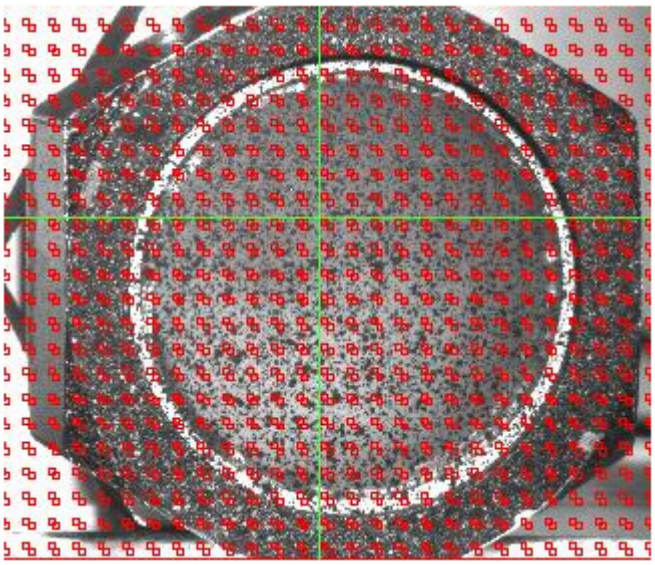

Figure 3-2: A DIC image of a blister test on Gore-Select® series 57 shown with facets overlaid

After the software solved all of the readable data points within the blister, a measurement of curvature was needed to obtain stress values using thin-wall pressure vessel theory as described in Eq. (3.1). In order to efficiently obtain these values on a large volume of data, a best-fit sphere was used to model all available data points in each frame. Clearly, a spherical fit of the blister in the first few images is a poor approximation since the radius of curvature is infinite for a flat object. As the blister grows, the spherical fit becomes much more accurate and enables efficient and reasonable biaxial stress estimates. We note that Hencky's solution indicates that only the central portion of the blister experiences the equal biaxial stress state characteristic of a spherical cap. However, locating the true center of each blister from specimen to specimen is not feasible. In order to maintain consistency from sample to sample, the entire data set is used in the spherical fit. Although this method does induce some error, it was determined that a consistent analysis was more critical than minimizing the error in radius of curvature values. Initial investigations in which the fit region is hand-selected have shown no significant difference in radius of curvature values. Thus, for all blister geometries solved by the DIC, the engineering stress histories were created using Eq. (3.1) where the radius of curvature values were calculated from the best-fit sphere outlined. A sample of deflection data from the DIC is shown in Figure 3-3 along with the sphere of best fit for this data set.

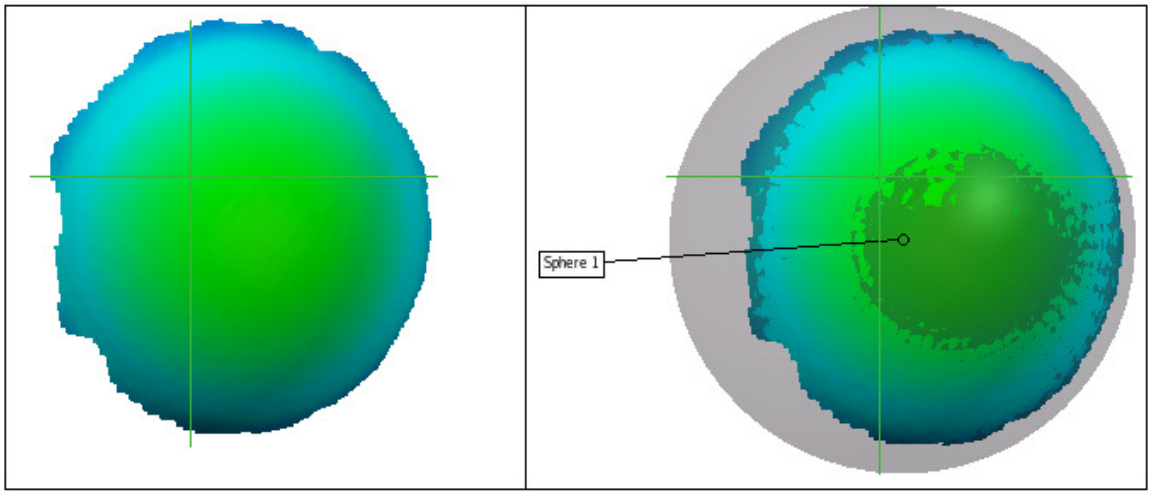

Figure 3-3: DIC deflection data for a blister test on Gore-Select® series 57 shown with the sphere of best-fit for the data

Blister stress histories were also calculated using Eq. (3.2) and the methodology presented in [31], as well as through a finite element model in ABAQUS. An axisymmetric shell model consisting of 400 SAX1 elements was used in conjunction with a linear viscoelastic constitutive model as used in [31] obtained using procedures from [20]. In defining this material model in ABAQUS, bulk and shear modulus values are needed as a function of time for the reference temperature of interest. Since no direct measurements were made to obtain these properties, assumptions were made in order to use the obtained uniaxial tensile stress relaxation modulus to generate the appropriate input. Specifically, the bulk modulus was assumed to relax significantly less than the shear modulus and was thus defined as a constant value. This common and reasonable approximation holds true for rubbery polymers above their glass transition temperature since the value of Poisson's ratio is approaching 0.5. Furthermore, the shear modulus was assumed to relax on the same time scale as the tensile stress relaxation modulus. From these assumptions, the material input for the model was fully defined given an instantaneous elastic modulus E, initial Poisson's ratio v, and Prony series modulus coefficients with reference temperature specific relaxation times to define the relaxation phenomenon.

Since the FEA model has the ability to incorporate thickness changes within the membrane, thereby providing true stress values within the blister, the thickness values at each step were used to convert true stress values into engineering stress values. This was a necessary step in order to compare the three different methods since the DIC methodology and the linear viscoelastic analog to Hencky's solution have no direct means of addressing localized thinning in the membrane.

The procedures outlined above enable a measured deformation-based stress analysis procedure in addition to two different material property dependant procedures. First, we will examine the effects of the sample speckling process by comparing mechanical lifetimes among painted and unpainted samples. Differences here would suggest that the sample preparation

has a significant effect on the observed behavior. Subsequently, the three stress analysis methods will be compared. Agreement among methods will validate the concept of extending small strain, uniaxially obtained material properties into the biaxial stress state of the blister which is more representative of conditions within fuel cell applications.

Results and Discussion

As a first step in quantifying the effect of the paint speckling procedure on the mechanical durability of the membrane, lifetime results from the painted specimen were compared to those results published in [31]. Since the tests were conducted on different size ferrules, pressure ramp rates could not be used as the benchmark. Instead, drawing on conclusions from [13], applied stress rates were calculated using Hencky's solution, so that a direct comparison could be made. Additionally, constant pressure test data from [14] were compared to constant pressure test data on painted specimens from this study. As seen in the ramped pressure comparison of Figure 3-4 and the constant pressure comparison of Figure 3-5, although the painted specimens exhibit more scatter than do unpainted specimens and perhaps show some lessened durability, the lifetimes do not appear to be so significantly affected as to warrant concern. Since strength is based on localized details of the membrane, the increased scatter with painted specimen is not surprising.

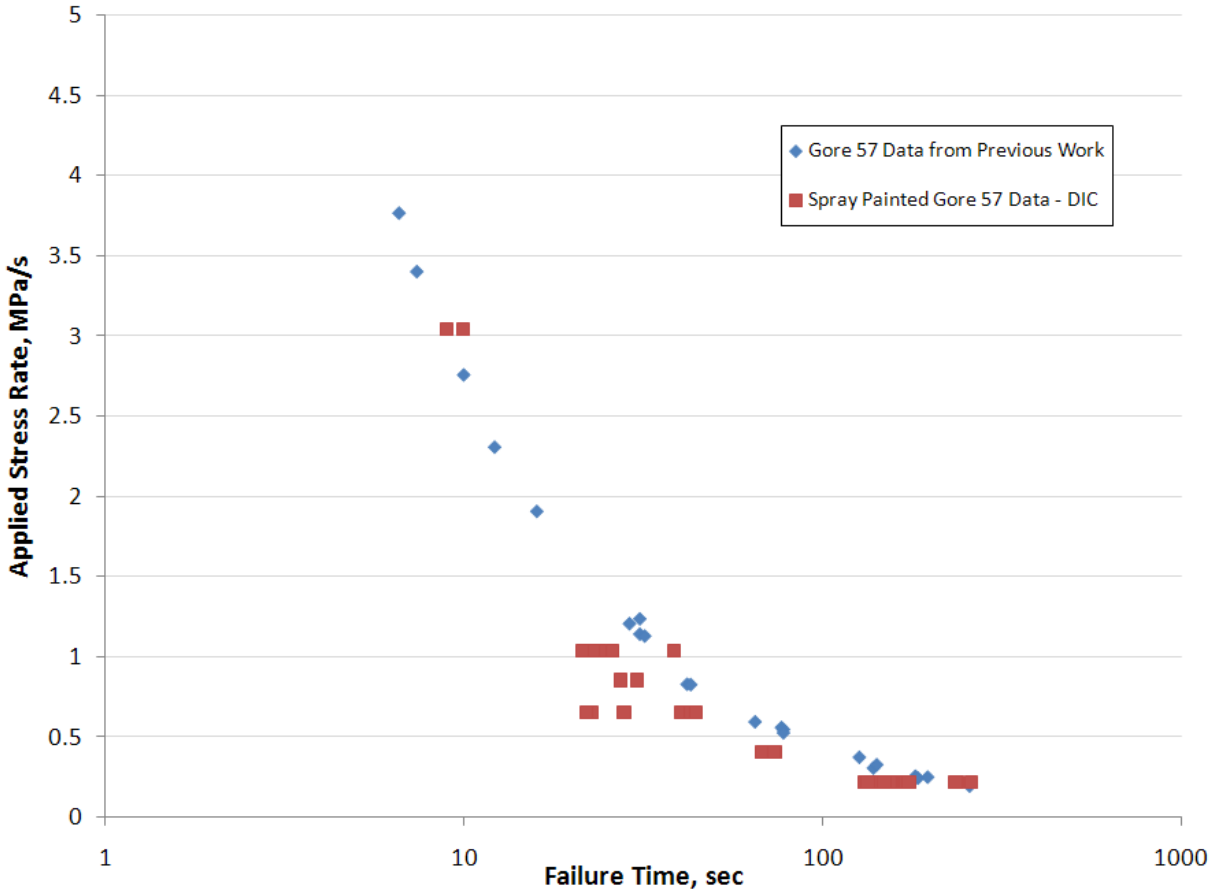

Figure 3-4: Comparison of unpainted and painted Gore-Select® series 57 lifetimes in ramped pressure testing at 90 °C to quantify effect of paint speckling on the mechanical durability of the membrane

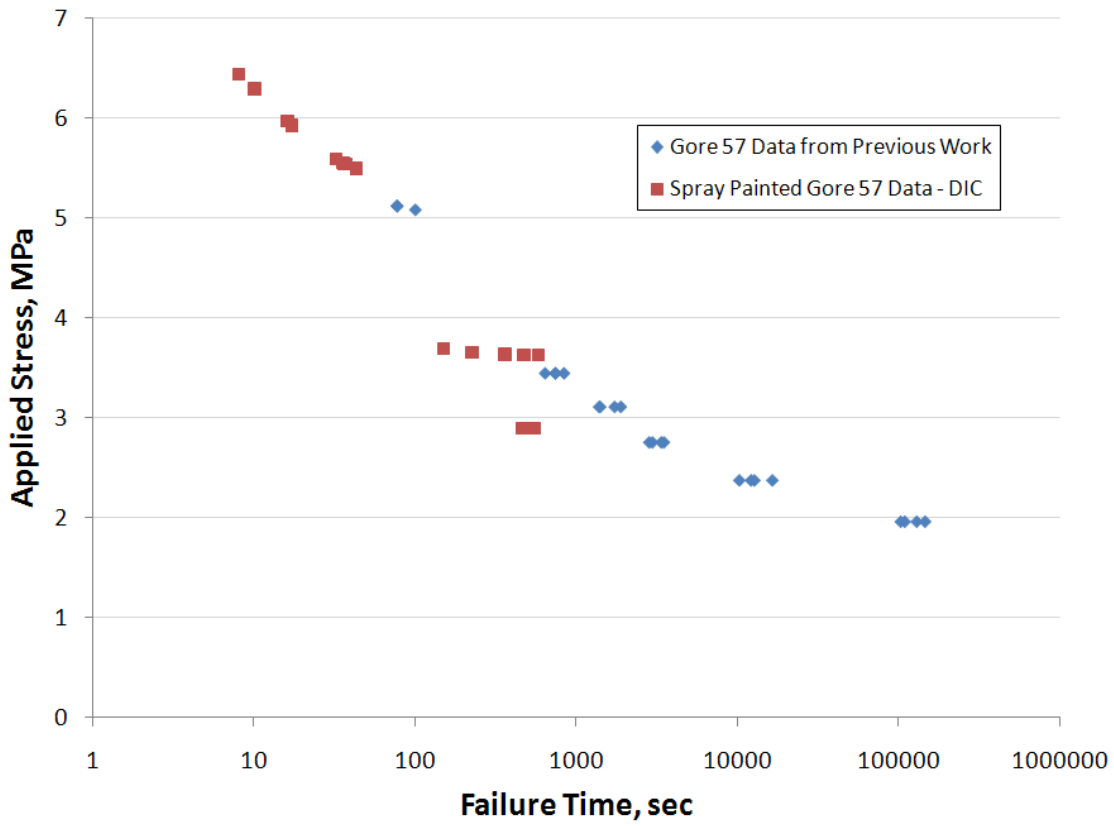

Figure 3-5: Comparison of unpainted and painted Gore-Select® series 57 lifetimes in constant pressure testing at 90℃ to quantify effect of paint speckling on the mechanical durability of the membrane

Next, the DIC system was used to determine best-fit spheres and radius of curvature values for each trial at varied pressure ramp rates and constant pressure values. These radius of curvature values were used in Eq. (1) to calculate stress histories for each trial. The results were reasonably consistent from test to test, especially for higher pressure ramp rates. In Figure 3-6, stress histories for pressure ramp rates of 0.1 kPa/s and 1 kPa/s are shown to demonstrate this encouraging consistency. Stress histories for constant pressure testing also showed consistent results and sample data collected at pressure values of 14 kPa, 20 kPa, and 24 kPa are shown in Figure 3-7.

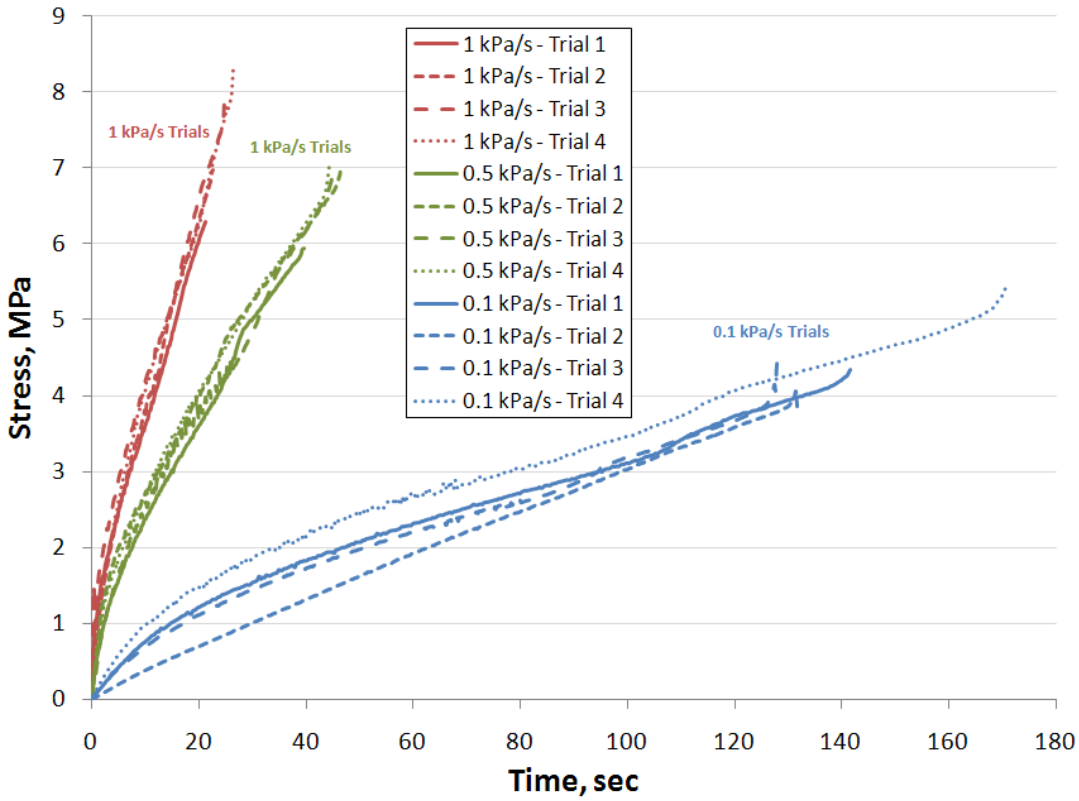

Figure 3-6: Stress histories calculated from DIC best-fit sphere data for ramped pressure testing at 90℃ on Gore-Select® series 57 membrane at pressure ramp rates of 1 kPa/s, 0.5 kPa/s, and 0.1 kPa/s

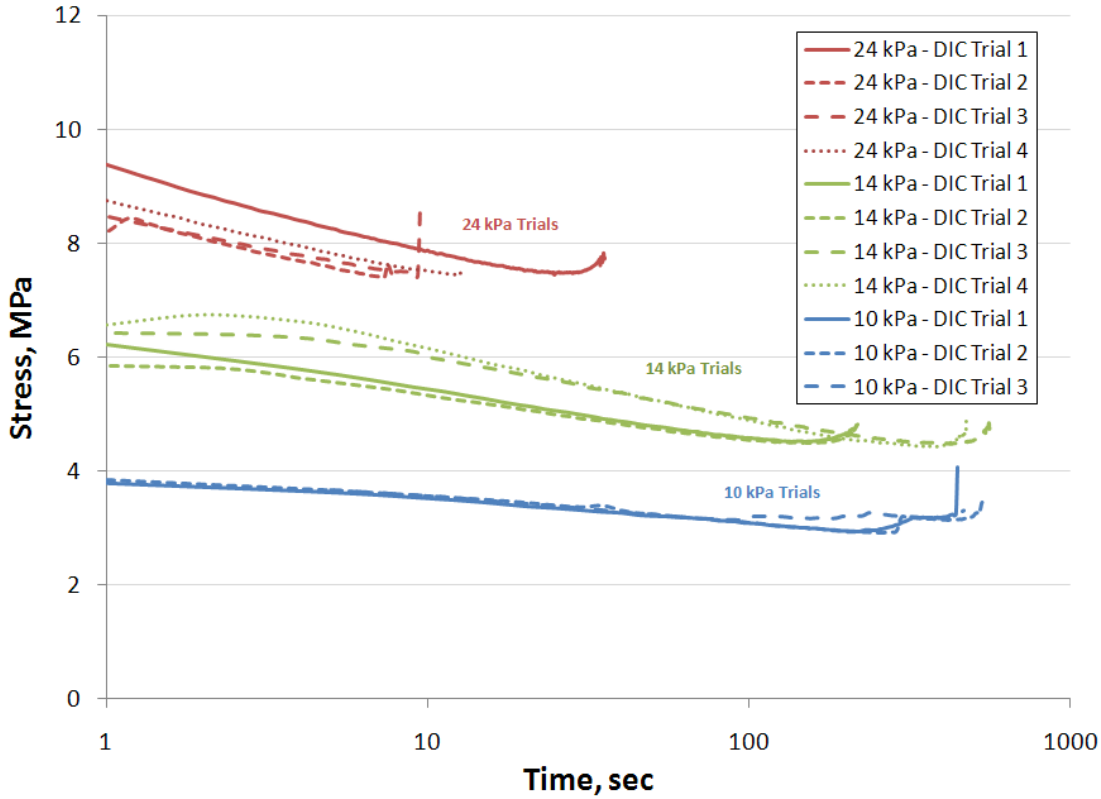

Figure 3-7: Stress histories calculated from DIC best-fit sphere data for constant pressure testing at 90℃ on Gore-Select® series 57 membrane at applied pressures of 10 kPa, 14 kPa, and 24 kPa

The encouraging consistency in the DIC work led to stress history comparisons between the material model independent DIC work, and the two constitutive based analysis methods of the linear viscoelastic analog to Hencky's solution and the FEA model. In the ramped pressure case, good agreement is found among all three methods as shown in Figure 3-8 (a), (b), and (c). This not only serves to validate the use of the linear viscoelastic constitutive model in this work, but also suggests that both of the model dependant stress analysis methods used are corroborated by the DIC measurements. This encouraging agreement provides additional validation to the methodology and conclusions of [31].

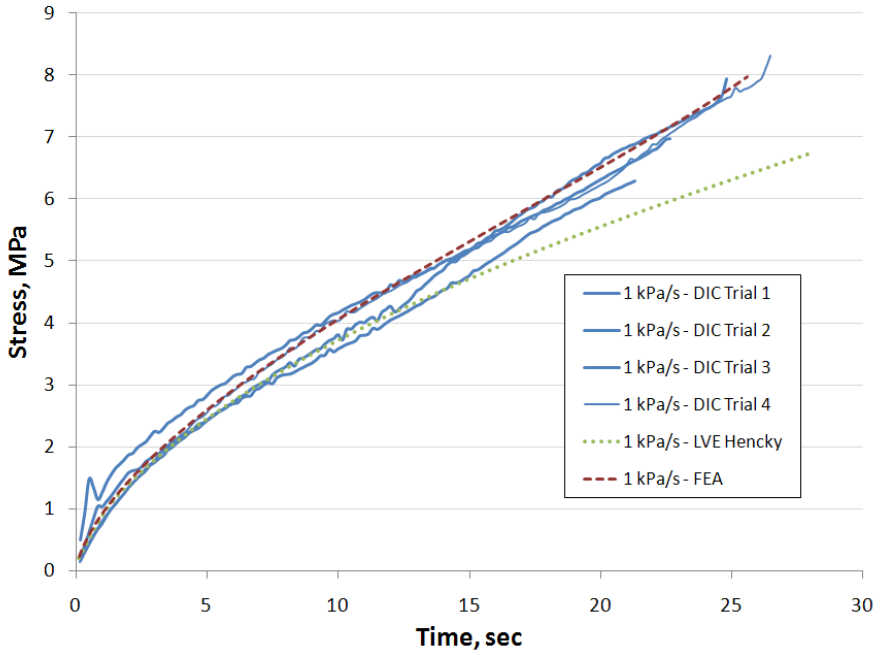
Stress, MPa
Time, sec
1 kPa/s - DIC Trial 1
1 kPa/s - DIC Trial 2
1 kPa/s - DIC Trial 3
1 kPa/s - DIC Trial 4
1 kPa/s - LVE Hencky
1 kPa/s - FEA

(a)

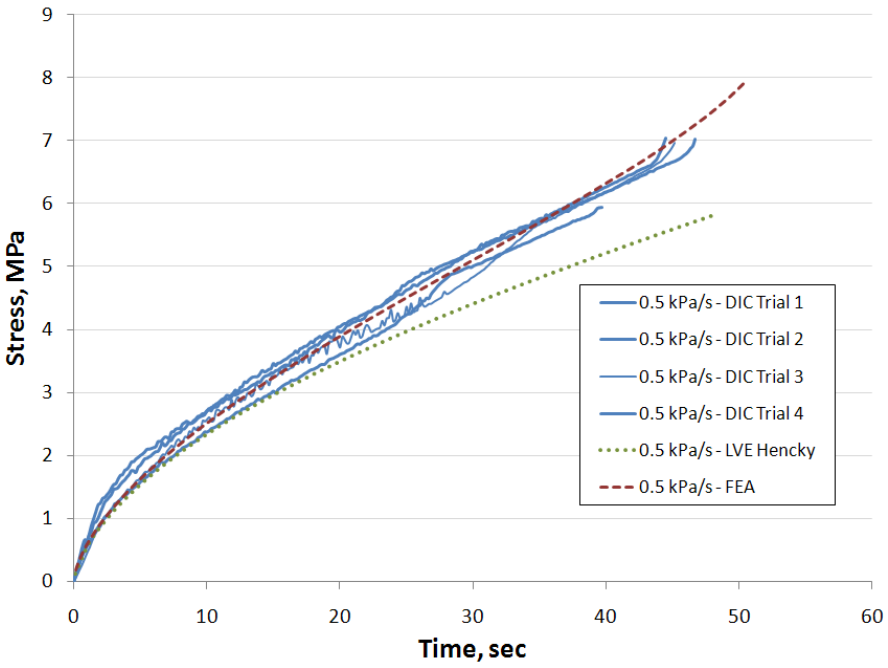
Stress, MPa
Time, sec
0.5 kPa/s - DIC Trial 1
0.5 kPa/s - DIC Trial 2
0.5 kPa/s - DIC Trial 3
0.5 kPa/s - DIC Trial 4
0.5 kPa/s - LVE Hencky
0.5 kPa/s - FEA

(b)

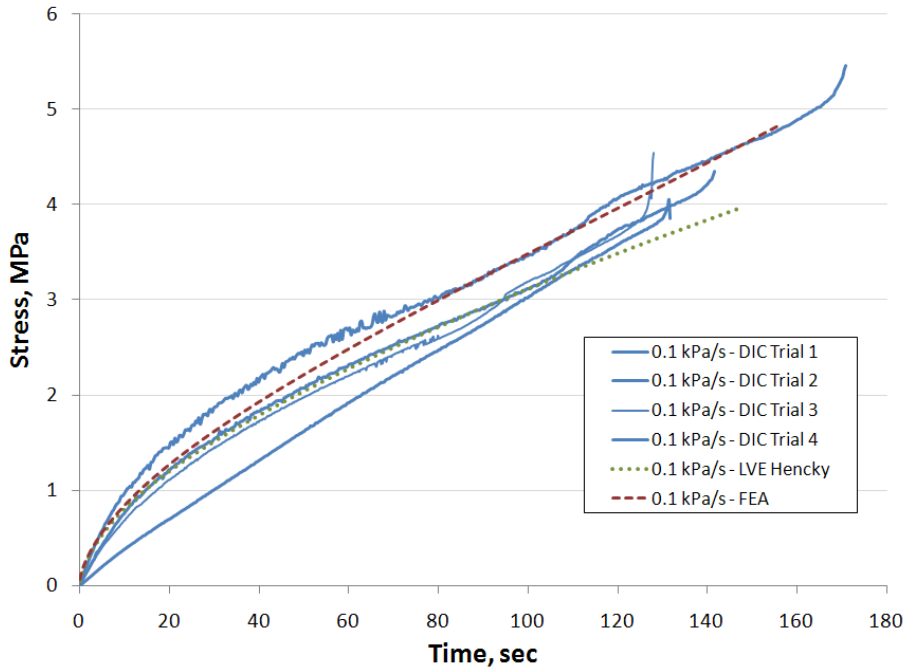

(c)

Figure 3-8: Comparison plot of DIC, LVE Hencky, and FEA stress analysis method for ramped pressure testing at 90℃ on Gore-Select® series 57 membrane at pressure ramp rates of (a) 1 kPa/s, (b) 0.5 kPa/s, and (c) 0.1 kPa/s

In studying Figure 3-8, it is clear that the LVE Hencky solution is consistently lower than the FEA solution. Furthermore, it appears that in the 1 kPa/s and 0.5 kPa/s ramp rates, the DIC measurements suggest that the FEA solution is more accurate than the LVE Hencky solution. It is somewhat expected that the FEA solution would provide more accurate results since it is better able to incorporate nonlinear geometric effects in the solution while the Hencky solution can only handle moderate geometric nonlinearity. However, it is difficult to make any definitive claims of one solution method being better than the other since the scatter in the DIC data is on the same order of the difference between the LVE Hencky and FEA solutions. A similar stress analysis comparison is showed for the constant pressure test results in Figure 3-9 (a), (b), and (c).

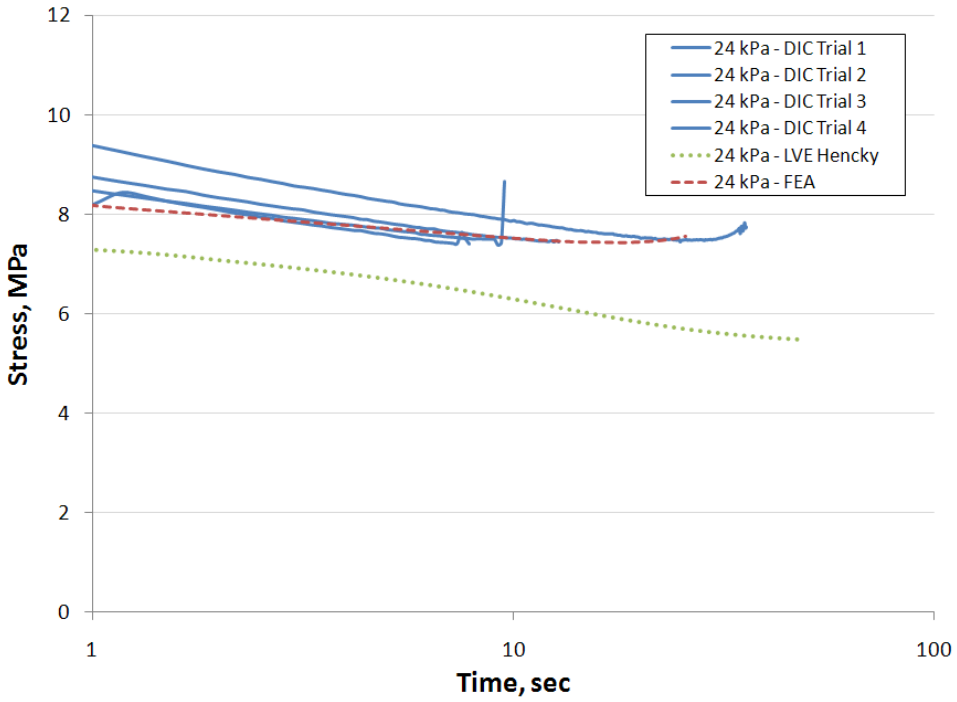
12
10
8
6
4
2
0
Stress, MPa
1
10
100
Time, sec
24 kPa - DIC Trial 1
24 kPa - DIC Trial 2
24 kPa - DIC Trial 3
24 kPa - DIC Trial 4
24 kPa - LVE Hencky
24 kPa - FEA

(a)

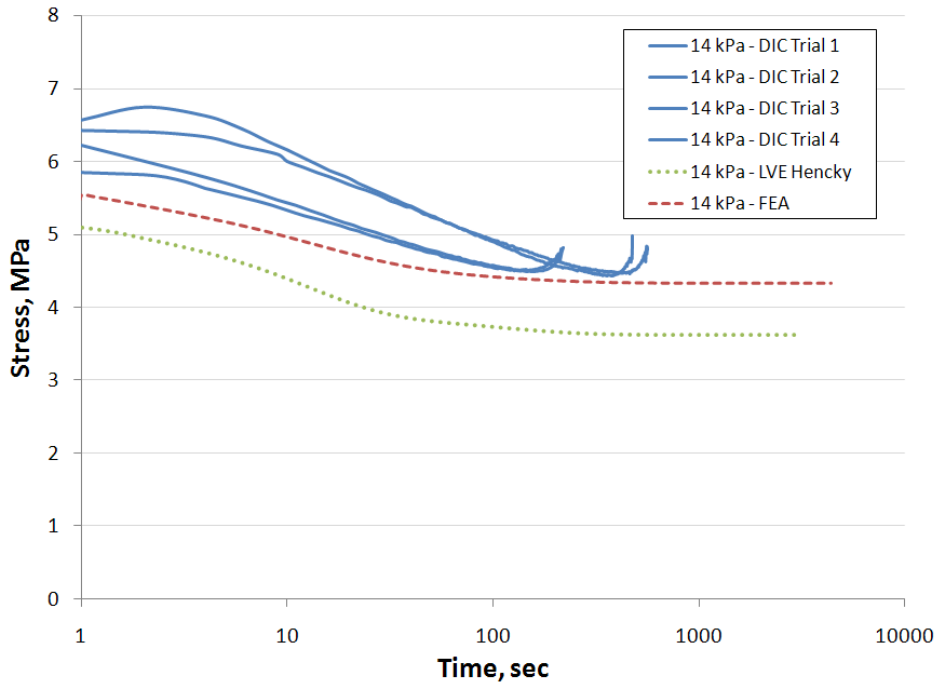
8
7
6
5
4
3
2
1
0
Stress, MPa
1
10
100
1000
10000
Time, sec
14 kPa - DIC Trial 1
14 kPa - DIC Trial 2
14 kPa - DIC Trial 3
14 kPa - DIC Trial 4
14 kPa - LVE Hencky
14 kPa - FEA

(b)

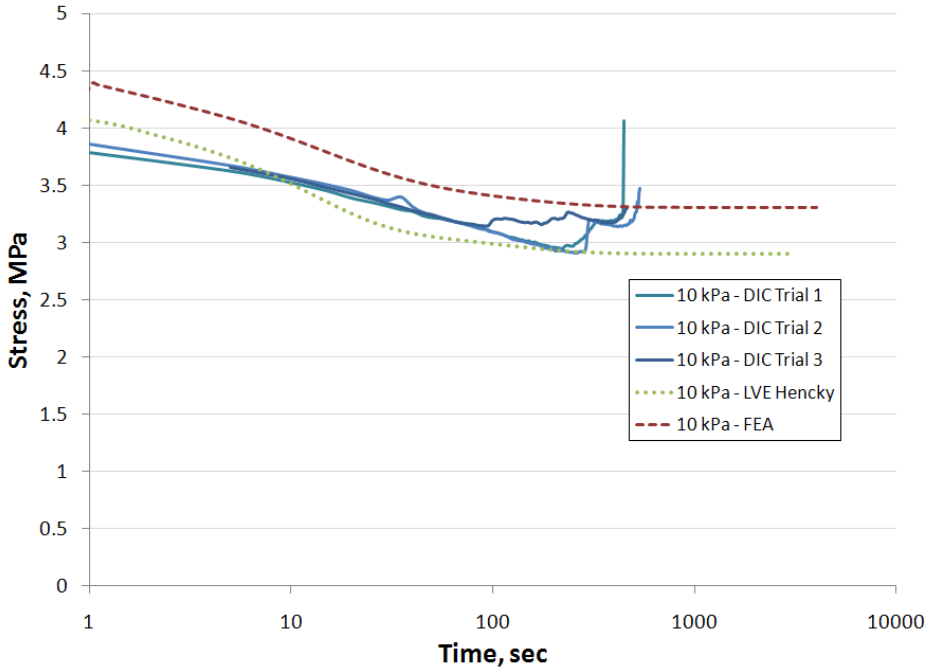

(c)

Figure 3-9: Comparison plot of DIC, LVE Hencky, and FEA stress analysis method for constant pressure testing at 90℃ on Gore-Select® series 57 membrane at pressure set points of (a) 24 kPa, (b) 14 kPa, and (c) 10 kPa

From Figure 3-9 it is seen that the discrepancy between the LVE Hencky solution and the FEA results for the constant pressure case is more pronounced than the ramped pressure case. The DIC measurements consistently agree with the FEA results across all pressure levels. However, the FEA results do appear to provide stress values slightly lower than the DIC data suggests. The cause for this discrepancy is currently under investigation. It is possible that this phenomenon appears because the simple linear constitutive model being used is not sufficient to completely model the behavior of a blister test involving biaxial loading and large strains.

Overall, the agreement between the DIC calculated stress histories and the FEA model results is very encouraging. The consistency between a geometric, measurement-based analysis with a material model dependent method serves to validate the extension of the uniaxially obtained, small strain-based, linear viscoelastic constitutive model into a bixially loaded, large strain application. This is a critical step in evaluating the appropriateness of using linear viscoelastic material modeling to calculate the environmentally induced stresses that are experienced by the PEMs during actual fuel cell operation. On another level, this study serves to validate the LVE Hencky method of stress analysis for the ramped pressure case as used in [31]. Although this method was less accurate in the constant pressure case, the error was reasonable and it could be considered a rough first order approximation due to its ease of development. Furthermore, the consistency among the methods provides a solid base of stress analysis tools necessary to developing a robust lifetime prediction model for these membranes tested under biaxial loading conditions. This is the focus of an ongoing study.

Conclusions

Pressure loaded blister tests were used in conjunction with the DIC system to analyze biaxial stress histories under ramped and constant pressure loading conditions. Since the DIC measurement methodology requires paint speckled membranes, lifetime comparisons of painted and unpainted membranes were compared. It was determined that the paint had no significant impact of the material lifetimes observed aside from an increase in scatter of the data. The blister stress histories calculated from the DIC showed good agreement with both the FEA and LVE Hencky methods of stress analysis. This consistency among methods validated the extension of the constitutive model obtained using small strain, uniaxial testing into applications involving both large strain and biaxial loading. Having validated both the constitutive model and the FEA modeling of the blister, efforts can progress towards the goal of developing a lifetime prediction model capable of predicting membrane failure due to biaxial stresses induced in the membrane due to hygrothermal environmental fluctuations. These works are ongoing and remain one of the critical elements required to apply ex-situ testing such as the pressure-loaded blister test and to enhance our understanding of the conditions and mechanics of membrane behavior during the operation of fuel cell applications.

Acknowledgements

The authors are grateful to General Motors Corp, for sponsoring and supporting this research and to the Department of Engineering Science and Mechanics and the Department of Mechanical Engineering at Virginia Tech for providing facilities and fostering interdisciplinary studies in fuel cell research. They also would like to acknowledge Tim Schmidt from Trilion Quality Systems for his training and ongoing support with the DIC system. EM also wishes to acknowledge the support of National Science Foundation Grant No. EEC-0552738.

Chapter 4: Development of Lifetime Prediction Models to Predict the Failure of Composite Proton Exchange Membrane Using Pressure Loaded Blister Tests

Abstract

In automotive applications, temperature and moisture fluctuations in proton exchange membrane (PEM) fuel cells impose biaxial stress states in the biaxially constrained PEMs. The strength of the PEMs and their ability to withstand stresses induced by the cyclic environment play an important role in membrane durability and consequently, fuel cell durability. In this study, pressure loaded blisters are tested until failure under both quasi-static constant pressure loading and cyclic pressure-controlled fatigue for a representative composite PEM, Gore-Select® Series 57. Finite element (FE) simulations of the experimental tests are used to generate stress histories for each testing mode. Experimental data and FE generated stress histories of the quasi-static constant pressure tests are used to develop linear damage accumulation and residual strength based lifetime prediction models. The models are then implemented using fatigue stress histories to predict fatigue failure times of the blister tests. Successful demonstration of these lifetime prediction models suggests that the models could predict failure times under any given stress history whether mechanically or environmentally induced. Validated prediction models could make it possible to predict the lifetime of PEM fuel cells in automotive applications as a function of known operating conditions and the constitutive behavior of the PEM.

Introduction

Durability of the proton exchange membrane (PEM) used in fuel cell transportation applications remains a critical issue. The Department of Energy (DOE) has determined that fuel-cell stacks will need lifetimes reaching 5000 hours to compete with the current light vehicle standards. In an effort to steadily progress towards this eventual goal, the DOE has established a 2000 hour lifetime benchmark in 2009 [37]. Although many factors contribute to the overall durability of the PEM, studies have shown that membrane failures are often characterized by mechanically driven propagation of localized defects [38]. Furthermore, the harsh hygrothermal environment of the operating fuel cell has been shown to cause local stress concentrations in the membrane which would significantly contribute to the propagation of the localized defects [39]. From this work, it is clear that a better understanding of the mechanical integrity of PEM could lend insight into the fuel cell durability issue and help the industry further progress towards the DOE milestones.

A novel method of investigating these mechanical issues within the PEM was introduced, which focused on a biaxial stress state via pressurized blister tests rather than the more traditional uniaxial tensile test methods [13]. It is believed that biaxial strength methods may be a more applicable analog to the stress states imposed by temperature and humidity fluctuations within a live fuel cell. Initial work led to the collection of characteristic biaxial strength as a function of time and temperature for various commercially available membranes tested under ramped pressure, constant pressure, and cyclic fatigue conditions [14, 31, 40]. While these characterizations may prove useful in a laboratory setting, the loading conditions are more

simplified than the loading histories expected of an operating fuel cell. However, success has been demonstrated in developing models for various viscoelastic materials which use experimental data collected under simplified loading conditions to predict failures of the material under more complex loading histories [41-43].

One widely used model for predicting fatigue lifetimes is the Palmgren-Miner cumulative damage rule [44] which bases specimen failure on a damage parameter, *D*. Initially, a specimen is undamaged, *D=0*, and proceeds to accumulate damage throughout the loading history. In the case of fatigue, the cumulative damage is given by

$$D = \sum_i d_i = \sum_i \frac{n_i}{N_i} \tag{4.1}$$

where d_i is a damage fraction, n_i is the number of cycles spent at a particular loading amplitude, and N_i is the number of cycles to failure if the specimen were only loaded at that particular loading amplitude. The failure of a specimen occurs when the summation of the damage fractions is equal to unity. The natural analog to this rule for creep loading is the linear damage accumulation rule (from here on referred to as LDA) and is given by

$$D = \sum_i d_i = \sum_i \frac{\Delta t_i}{\tau_i} \tag{4.2}$$

where Δt_i is the amount of time spent at a specific stress level and τ_i is the time to failure at that given stress level. In keeping with the Palmgren-Miner rule, specimen failure is defined as the time at which the damage fractions sum to 1.0. Although initially defined discretely, Eq. (4.2) can be easily rewritten as an integral for increasingly small values of Δt_i,

$$D = \int \frac{dt}{\tau} \tag{4.3}$$

where τ is a continuous function of the applied stress over the interval of interest. Although there is much debate on the validity of LDA for many applications, it still remains one of the most widely used lifetime prediction models for design and its simple methodology allows for quick, and often surprisingly accurate, damage model development.

Another family of lifetime prediction models is based on the introduction of a material parameter that is the residual strength of the material. This parameter is conceptualized as the remaining strength left in the material at any instant in time with the initial value being equal to the ultimate strength of the material. It has been noted that many forms proposed for the differential equation governing the residual strength are just generic forms of the generalized rate equation where the residual strength is given as a monotonically decreasing function with time [45]. In general, the residual strength is governed by

$$\frac{d\sigma_r}{dt} = -\beta \frac{\alpha t^{\alpha-1}}{\gamma \sigma_r^{\gamma-1}} \tag{4.4}$$

where σ_r is the residual strength, t is time, and α,β,γ are material parameters. Failure in this model is defined as the time at which the remaining residual strength is less than or equal to the applied stress. By applying the initial condition of $\sigma_r(0) = \sigma_{ult}$ and the failure criterion of $\sigma_r(t_f) = \sigma_a(t_f)$ and integrating, this can be written as

$$\sigma_r(t)^\gamma = \sigma_{ult}^\gamma - \frac{\sigma_{ult}^\gamma - \sigma_a(t)^\gamma}{\sigma_a(t)^\gamma} \frac{t}{\tau} \tag{4.5}$$

where $\sigma_r(t)$ is the residual strength as a function of time t, $\sigma_a(t)$ is the applied stress as a function of time, σ_{ult} is the ultimate strength of the material, γ prescribes the shape of the σ_r versus t curve, and τ is the time to failure associated with an applied constant stress. One of the advantages of the residual strength (hereafter referred to as RS) based approach is the physical significance of the residual strength parameter. While quantifying dimensionless damage can be somewhat ambiguous, a parameter describing the static strength left in a specimen allows for a more comprehensive understanding of material degradation throughout a given loading history.

Ultimately, the development of a robust lifetime prediction model would prove invaluable to fuel cell durability studies and the progression towards DOE targets. As an initial step in this direction, the focus of this study is to use constant pressure blister test data collected at 90°C on Gore-Select® series 57 data to develop LDA and RS models, make predictions of simple cyclic pressure fatigue tests, and validate with experimental fatigue data.

Model Development Procedure

Lifetime prediction model methodology is simple in principle. Given knowledge of the stress-life curve of a material (analogous to an S-N curve in fatigue) and an arbitrary stress history, the model will predict the subsequent time to failure. In this study, however, the development of the model is more complex due to the nature of the blister test. Constant pressure (hereafter referred to as CP) testing can be thought of as the blister test analog to uniaxial creep, although the stresses are clearly not constant throughout the test. Both the viscoelastic nature of the PEM as well as the geometric relaxation (decreasing radius of curvature) contribute to the overall variation in stress throughout the life of the test. Still, development of a lifetime prediction model from these constant pressure tests can still be accomplished using a combination of experimental data and finite element (FE) modeling. Assuming that the failure mechanism controlling constant pressure test failures is the same mechanism driving fatigue test failures, the lifetime prediction model developed for CP testing would be applicable to fatigue. The validity of this assumption can be explored by comparing experimental fatigue data to fatigue predictions. With these concepts in mind, the development methodology is outlined in greater detail below.

Collect data for CP and fatigue testing of Gore-Select® series 57

Data was collected at 90°C on Gore-Select® series 57 for CP tests ranging from 6, 8, 10, 12, 14, and 24 and fatigue tests ranging from 6, 7, 8.5, 9, 10, 11.5, and 12.5 kPa (duty cycle 10 seconds pressurized, 4 seconds unpressurized.) The data collected was previously published and for further information regarding experimental procedure, please see [46].

Run FE simulations to generate stress histories of CP and fatigue tests

FE simulations were performed using ABAQUS 7.1 in order to generate stress histories of the experimental data points. An axisymmetic shell model with 400 SAX1 elements was used to produce simulations mimicking the experimental tests. The shell thickness and model length were equal to the membrane thickness and experimental blister radius, respectively. Linear viscoelastic data as collected from stress relaxation tests on Gore-Select® series 57 was used as the input material characterization [20]. Since ABAQUS requires viscoelastic Prony series material characterization via bulk and shear relaxation modulus, it was assumed that the shear relaxation modulus, G_0 and G_i, occurs on the same time scale as the tensile relaxation modulus while the bulk relaxation modulus remains constant. Table 4-1 below shows the viscoelastic Prony series inputs used in the ABAQUS analysis for 90° C.

Table 4-1: Prony series coefficients used as viscoelastic characterization input for ABAQUS analysis simulations of Gore-Select® series 57 at 90°C

i	G_i	K_i	τ_i
0	11.29	52.69	(n/a)
1	0.0599	0	0.001
2	0.0598	0	0.01
3	0.0665	0	0.1
4	0.1237	0	1
5	0.3744	0	10
6	0.0638	0	100

The FEA model was used to generate predicted CP stress histories for 6, 8, 10, 12, 14, and 24 kPa of Gore-Select® series 57 at 90°C. These pressure levels were chosen specifically to correspond to the pressure levels for which experimental data was presented in [46]. Shown in Figure 4-1 is a plot of the FE stress histories obtained.

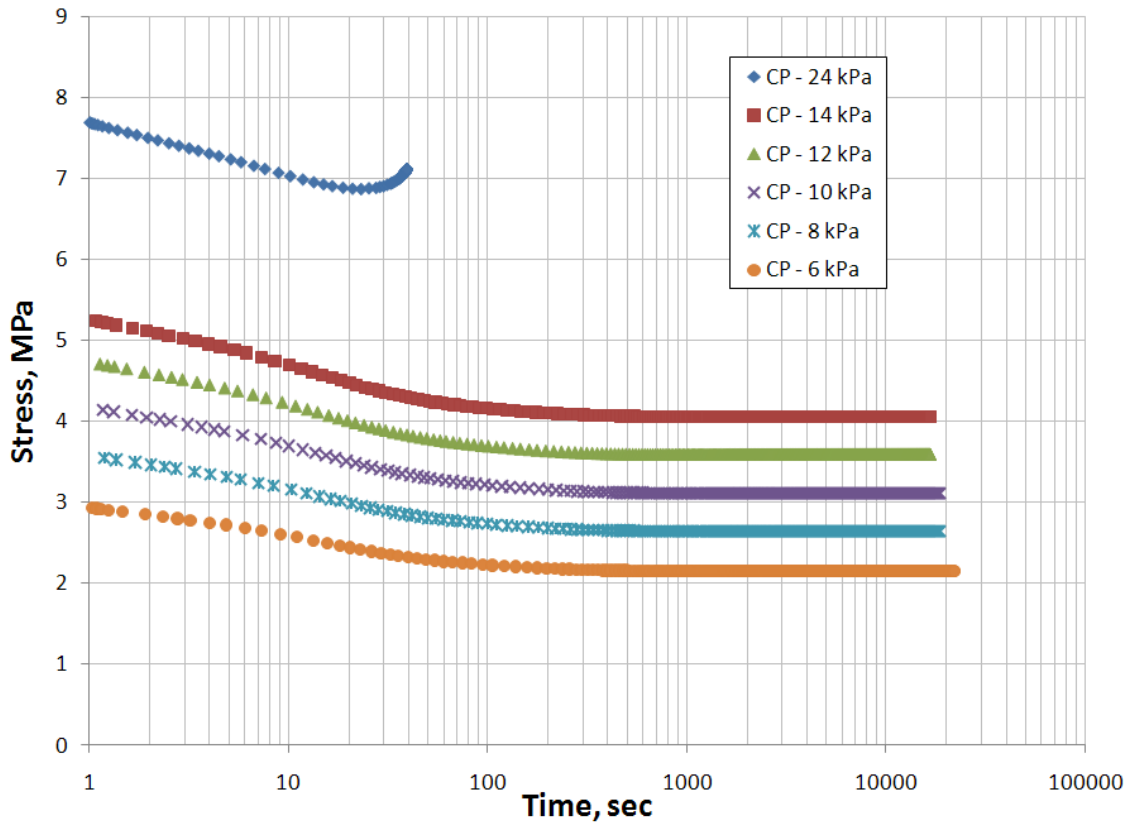

Figure 4-1: ABAQUS generated stress histories for the CP test cases needed to develop the lifetime prediction model at 90℃ for Gore-Select® series 57

Similar to the CP methodology, FEA results were generated for the fatigue tests. Simulations were performed at set pressure values of 6, 7, 8.5, 9, 10, 11.5, and 12.5 kPa using a 10-4 duty cycle (10 seconds of pressurization, 4 seconds of recovery time.) In Figure 4-2 below, the peak stress per cycle is shown for 6 kPa, 8.5 kPa, and 12.5 kPa.

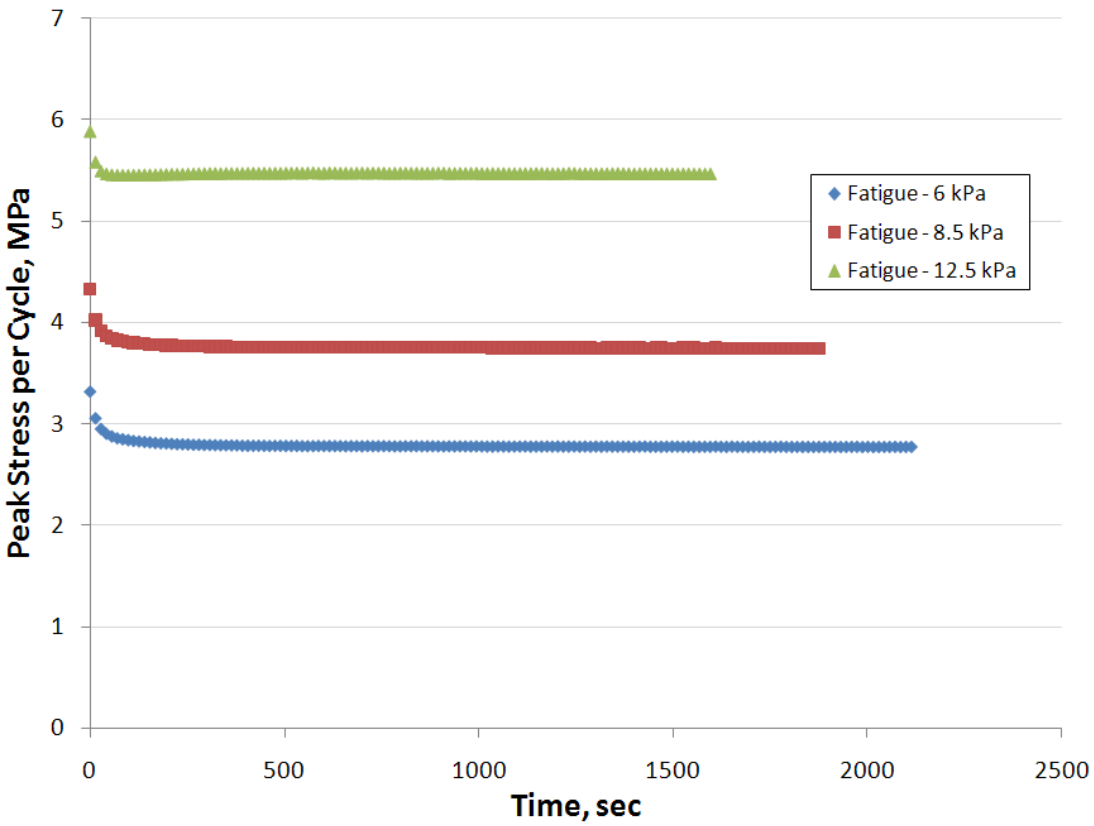

Figure 4-2: Peak stress per cycle plotted 3 select fatigue test cases needed to validate the lifetime prediction model at 90℃ for Gore-Select® series 57

The fatigue process becomes difficult for the FE model to handle at longer times due to repeated loading/unloading and excessive distortion of elements at the boundary. Because of this, the FEA histories tend to be much shorter than the timescale of the experimental failures observed. However, it appears that both the CP tests of Figure 4-1 and the fatigue tests of Figure 4-2 are reaching steady-state values. So that the model is not limited by the finite amount of data obtained by the FEA, the stress histories are assumed to continue indefinitely in their steady-state configuration.

Assume a power law form of the stress-life curve

One of the critical assumptions made in this study is an assumed power law form of the stress-life curve. This is to say that the time to failure τ, as a function of applied constant stress σ_a, can be written as $\tau(\sigma_a)=A\sigma_a^B$ where *A* and *B* are constants to be determined. These constants will be determined by choosing a damage evolution law and finding the best values of *A, B* which result in the least error between predicted lifetimes and experimental lifetimes of the CP experimental data. Once *A* and *B* have been determined, it is assumed that these values hold for any test exhibiting the same failure mechanism as in the CP tests.

Use LDA to solve for constants A,B

Using LDA to determine failure in a continuous loading history is described in general in (3). Introducing the assumed power laws for both the stress-life curve and the generalized CP stress history respectively, the equation is simplified to

$$D = \int \frac{dt}{\tau} = \int \frac{dt}{A\sigma_a{}^B} \tag{4.6}$$

where *A,B* are constants describing the stress-life curve, σ_a is the applied stress as a function of time, *t* is time, and failure is defined as the time at which *D*=1.

Since no mathematical fits to FEA CP stress histories proved accurate enough to warrant the simplification, a time marching algorithm was used with each output data set. The integration of Eq. (4.6) was performed numerically on each stress history until the model predicted failure. A program was developed in Mathematica in which the predicted lifetimes for a given *A,B* are calculated by the method above and then the error is determined by

$$Error = \sum_{\text{data of interest}} \left[\log\left(t_{f\text{predicted}}\right) - \log\left(t_{fe\text{xperimental}}\right)\right]^2 \tag{4.7}$$

The program enumerates the error based on each possible *A,B* pair within given intervals and the pair resulting in the least error gives the LDA developed values for *A,B*.

Use RS approach to solve for constants A,B

Using RS to determine *A,B* enjoys a similar programmatic approach as with LDA development. Lacking analytical methods of solving for *A,B*, the models of Eq. (4.3) and Eq. (4.5) must be implemented through another time marching algorithm where the residual strength is computed at each step in time along the given stress history. Failure is defined as the first time at which the residual strength is equal to or less than the applied stress. Given an arbitrary *A,B* pair, marching along the stress histories, the residual strength as a function of time and applied stress can be calculated by

$$\sigma_r(t) = \left[\sigma_{ult}^{\gamma} - \int_0^t \frac{\sigma_{ult}^{\gamma} - \sigma_a(t)^{\gamma}}{\sigma_a(t)^{\gamma}}\right]^{1/\gamma} \tag{4.8}$$

where the integral can be computed numerically using the trapezoidal rule between time steps of the stress history. In this study, σ_{ult} is assumed to be 30 MPa (an extrapolation from data in

[31]) and γ is assumed to be 1 since no data is available to suggest otherwise. A study to experimentally determine γ could improve the accuracy of this model.

Again, a Mathematica program was used in which the predicted lifetimes for a given *A,B* are calculated by the method above and then the error is determined by Eq. (4.8). The program enumerates the error based on each possible *A,B* pair within given intervals and the pair resulting in the least error gives the RS developed values for *A,B*.

Consistency check and model validation

It is important to make sure each developed model both provides consistent results when predicting CP tests (the same data points used in development) as well as model validation by predicting fatigue results with success. A model which provides CP predicted lifetimes consistent with the experimental lifetimes supports the validity of assuming a power law form of the stress-life curve. Predicting lifetimes from fatigue histories and comparing to experimental data is the first step in model validation. Further validation could be obtained from lifetime predictions of irregular loading histories and/or tests run at different temperatures and fatigue duty cycles. These other means are the focus of an ongoing study.

Results and Discussion

Both LDA and RS models were developed using the methodology outlined above. For the RS based model, *A*,*B* values were compared over the intervals of [0.1 x 10^6, 999 x 10^6] for *A*, and [-4.01,-8.01] for *B*. Table 4-2 below shows the calculated values of *A,B* for each respective model.

Table 4-2: Calculated A,B values for LDA and RS models respectively

	A	*B*
LDA	4.96 x 10^6	-4.69
RS	5.39 x 10^6	-4.01

Consistency checks were first performed on both models to ensure proper development and validity of assumptions before extending into fatigue predictions. Figure 4-3 and Figure 4-4 show the consistency checks for LDA and RS respectively.

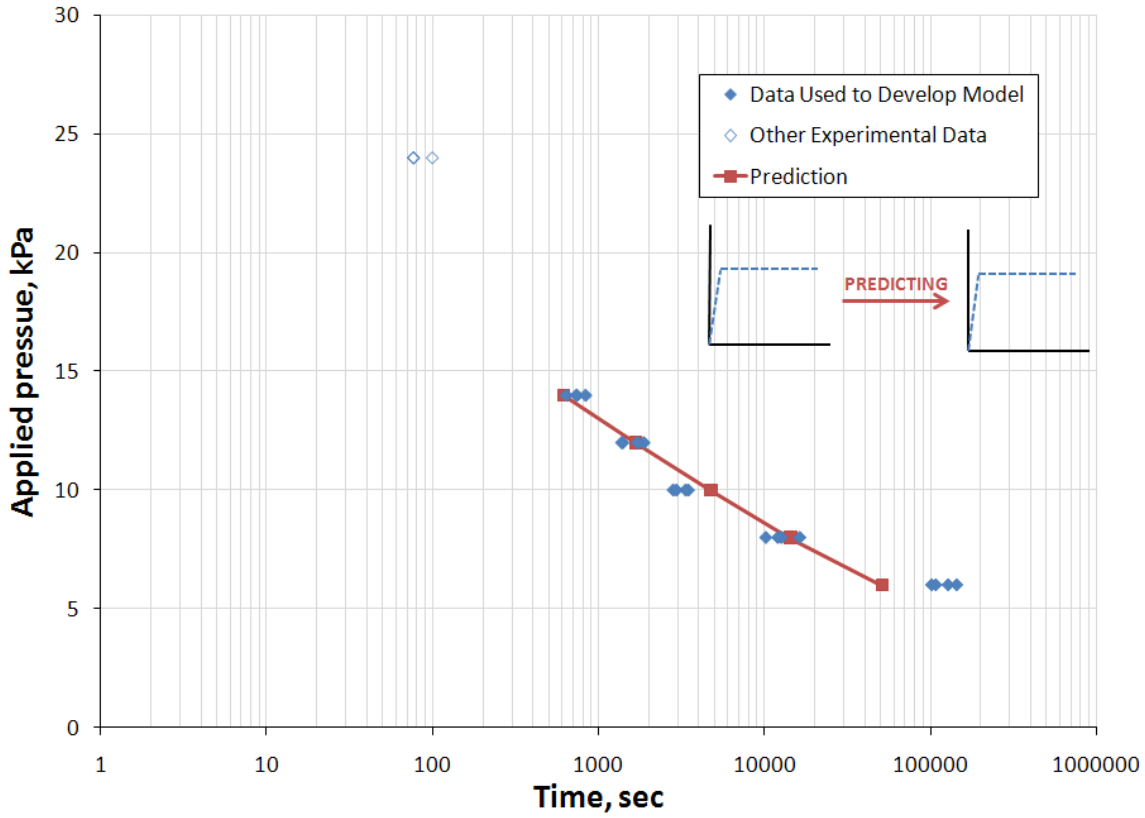

Figure 4-3: Consistency check for LDA development of Gore-Select® series 57 at 90°C

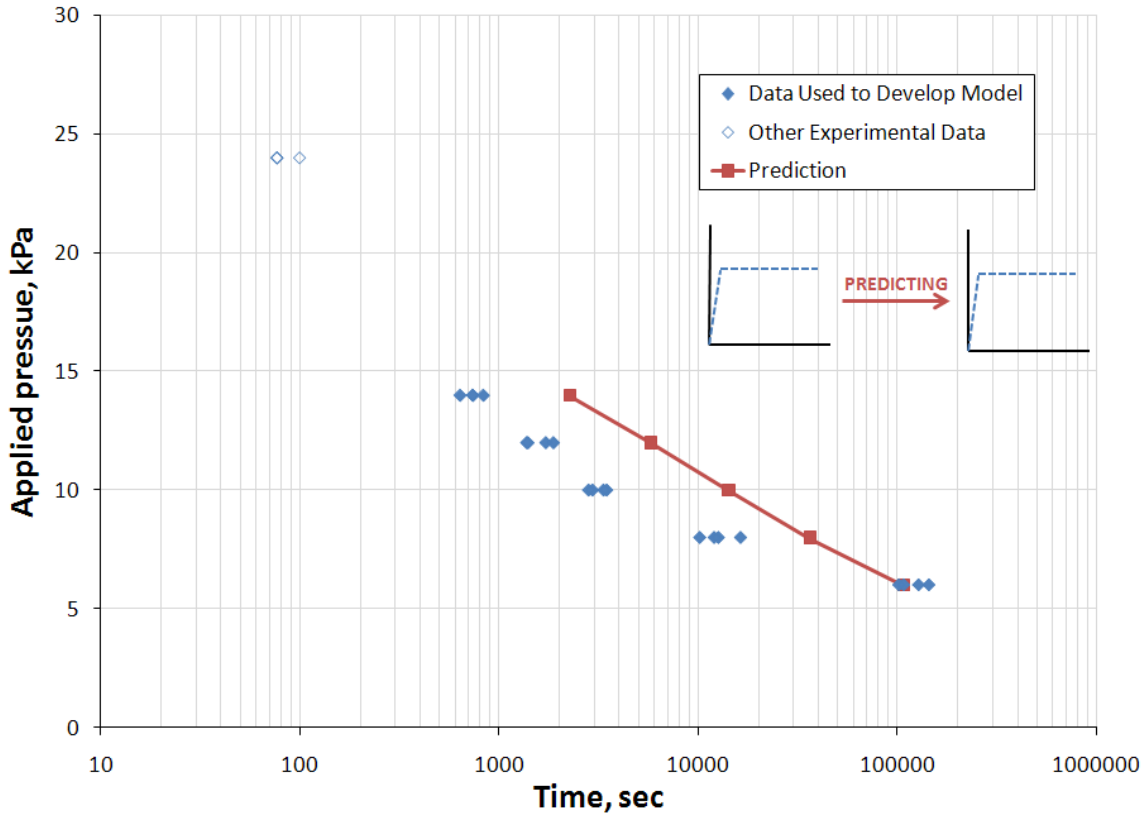

Figure 4-4: Consistency check for RS development of Gore-Select® series 57 at 90 ℃

Although the RS model consistency check is not nearly as accurate as the LDA model, this is still somewhat expected. Because this development uses an extrapolated value of the σ_{ult} and an assumption of γ=1, the RS model is very limited. However, further testing to explore appropriate values of these parameters would likely improve the accuracy of the model. Since both of these consistency checks look as expected, the next step is to make fatigue predictions and validate the model by comparing to experimental lifetimes. Comparison plots for fatigue predictions are shown in Figure 4-5 and Figure 4-6 for LDA and RS respectively.

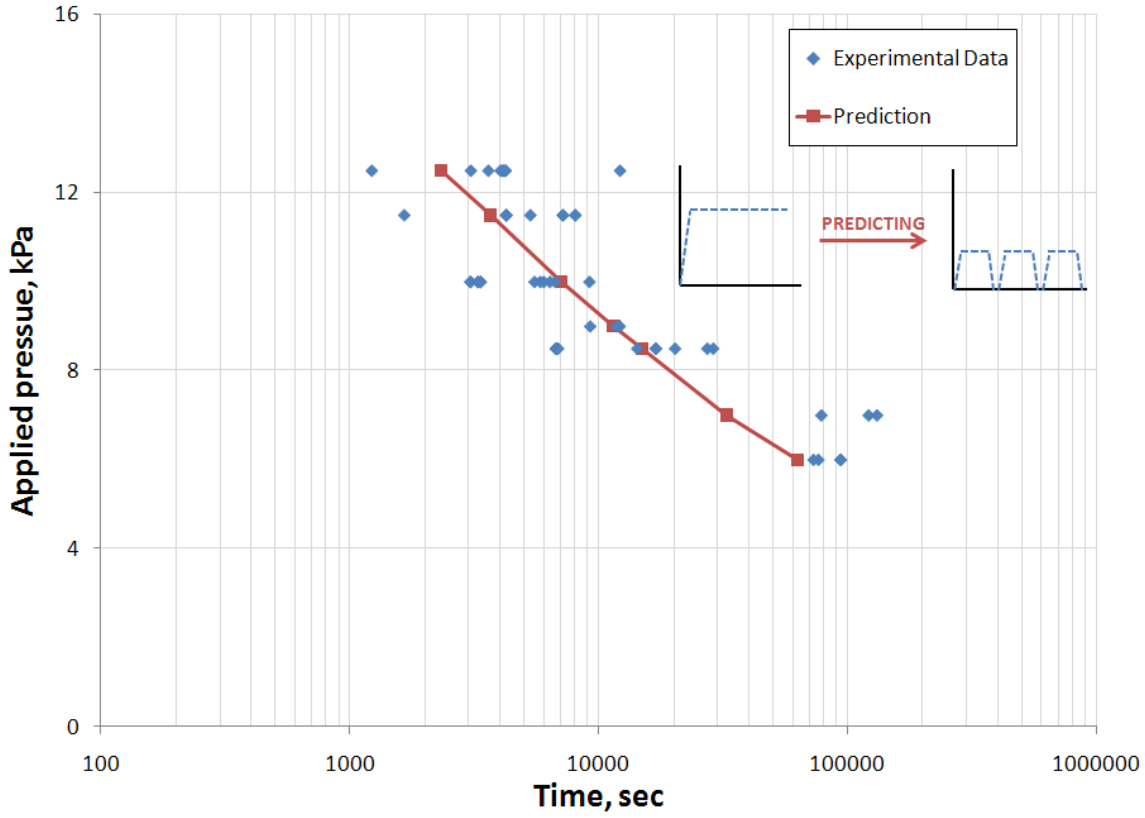

Figure 4-5: Fatigue prediction using the developed LDA model for Gore-Select® series 57 at 90℃

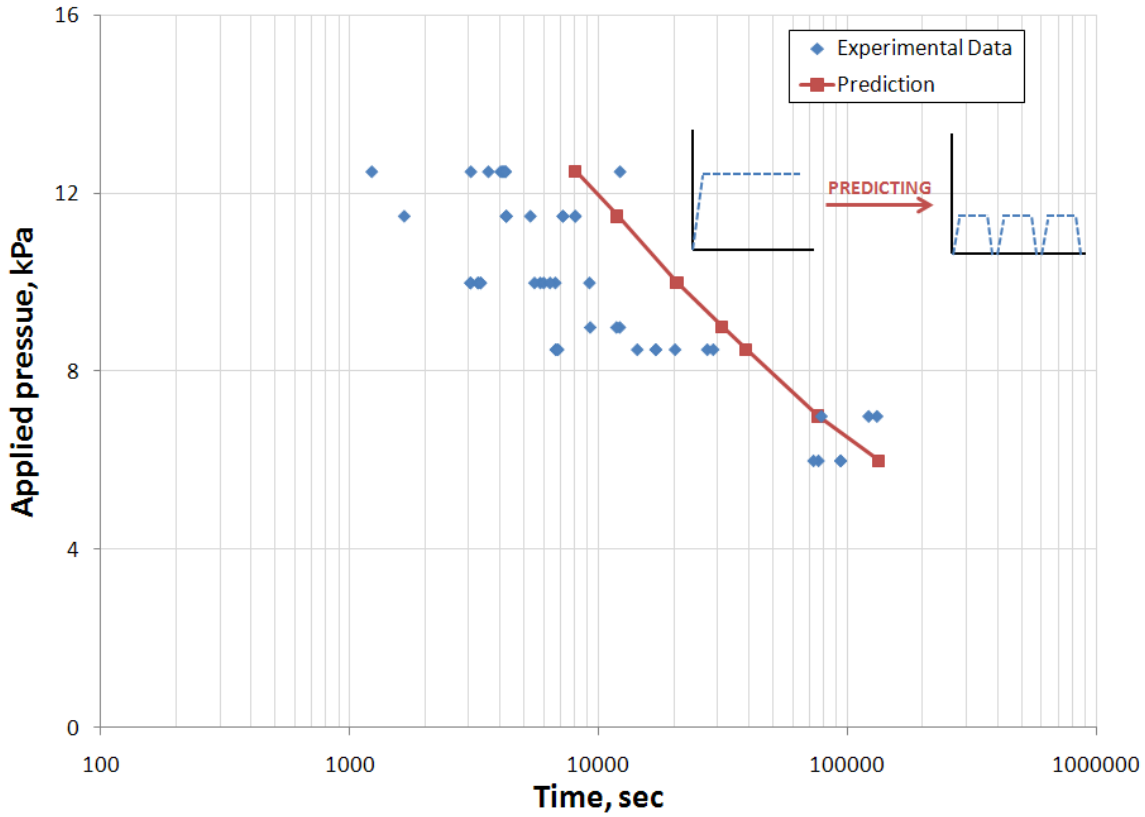

Figure 4-6: Fatigue prediction using the developed RS model for Gore-Select® series 57 at 90℃

Both LDA and RS models result in very encouraging predictions of the fatigue lifetimes. In particular, the LDA model consistently predicts failures within the scatter of the lifetime data. The RS model enjoys reasonable success in fatigue predictions, but tends to overestimate shorter lifetime tests. Overall, the LDA model clearly provides better results than does the RS model. However, since major simplifying assumptions for σ_{ult} and γ were made with the RS model, more data is needed to fully develop it and make a more robust comparison of the two models.

This demonstrated success of the models in predicting fatigue failures, encourages extension into different temperature regimes and more arbitrary loading conditions. If the models are further validated for these other cases, these simple lifetime prediction efforts could become an integral part of understanding PEM mechanical performance. Model development requires tests which, once perfected, could be completed in a matter of a few days. The ability to quickly analyze strength and lifetime differences from membrane to membrane would be particularly useful to the fuel cell industry as the technology progresses towards the DOE durability goals. Furthermore, if temperature and humidity operating conditions as recorded in test vehicle fleets can be successfully converted into equivalent stress histories, then validated lifetime prediction models would prove indispensible in determining appropriate service periods to avoid fuel cell stack failures.

Conclusions

Pressure controlled blister tests were performed to collect data on Gore-Select® series 57 at 90℃ loaded under both constant pressure (similar to uniaxial creep) and fatigue (periodically applied constant pressure levels) loading conditions. Finite element analysis was then used to translate the applied pressures into the stress histories which were paired with the experimental tests to develop lifetime prediction models. A linear damage accumulation model and a residual strength based model were chosen as the damage evolution laws of interest in this study. Both models were developed using the constant pressure test data and validated by agreement between predicted and measured lifetimes under fatigue. Future work will include extending these models to different temperatures as well as more arbitrary loading conditions. Further validation through these suggested extensions would provide a powerful tool for the fuel cell industry in the understanding of membrane durability.

Acknowledgements

The authors are grateful to General Motors Corporation for sponsoring and supporting this research and to the Department of Engineering Science and Mechanics and the Department of Mechanical Engineering at Virginia Tech for providing facilities and fostering interdisciplinary studies in fuel cell research.

Chapter 5: Conclusions

Conclusions

This section serves to summarize the overarching conclusions made throughout this thesis. It will be broken down into separate conclusions drawn in each of the 3 manuscripts followed by a brief “big-picture” approach.

Chapter 2 was dedicated to studying the time and temperature dependence of biaxial burst strength of Gore-Select® Series 57 proton exchange membrane. Specifically, pressure loaded blister tests were conducted over a variety of pressure ramp rates and temperatures and analyzed using a modified form of Hencky’s classical solution. The major conclusions of this study were:

- The elastic-viscoelastic correspondence principle was applied to Hencky’s classical linear elastic solution to obtain the linear viscoelastic analogous solution.
- Applying this LVE Hencky solution to collected data, biaxial burst strength values were obtained over a range of time/temperatures of interest. This data was used to form biaxial burst strength master curves.
- The temperature shift factors obtained from the construction of the biaxial burst strength master curves were compared to published temperature shift factors obtained in other testing modes and were found to be in reasonable agreement. This helps to validate the use of the time temperature superposition principle (TTSP) in this application.

Chapter 3 was dedicated to using the digital image correlation method to investigate the accuracy of the stress analysis methods used in previous and ongoing pressure-loaded blister work. The DIC methodology was studied with respect to mechanical durability and the measured deflections were used to compare to finite element analysis and LVE Hencky results for both ramped pressure and constant pressure tests. The major conclusions of this study were:

- The DIC methodology, which involves spray painting the membrane, was found to have no significant impact on the mechanical durability of the membrane. This suggests that this method should be appropriate to use for these durability focused, pressure loaded blister studies.
- Good agreement was demonstrated between measured DIC stress histories and the constitutive property dependent FEA and LVE Hencky analysis methods.
- The reasonable corroboration of all three methods serves to validate the extension of the small strain, uniaxially obtained constitutive model into the blister application which involves both large strains and biaxial loading.

Chapter 4 was dedicated to developing different lifetime prediction models capable of predicting blister failure of Gore-Select® Series 57 proton exchange membrane. Models were developed/calibrated using constant pressure test data and fatigue predictions/experimental results were used to validate the models. FEA stress histories were used as the stress analysis tool throughout Chapter 4. The major conclusions of this study were:

- Linear Damage Accumulation and Residual Strength based lifetime prediction models were developed. (Given any stress history input, the model will predict the associated failure time)
- The model, developed on constant pressure data, was validated by predicting experimental fatigue data with reasonable accuracy.

Overall, the conclusions from all manuscripts are encouraging advances in the study and understanding of membrane mechanical durability. Some overarching conclusions drawn from this entire work are:

- The characterization of biaxial strength/lifetime properties has been significantly advanced by the refined stress analysis methods discussed herein. While the LVE Hencky shows some discrepancies from FEA and DIC methods, it provides computationally cheap, reasonable first-order approximations. Applications requiring the utmost precision should utilize finite element analysis methods.
- The lifetime prediction model developed produces very encouraging results when used to predict fatigue results at the same temperature for which the model was developed. These results prompt extensions and further validation of the model by extending to other temperatures and more complex loading histories.
- The work with the DIC in this study has demonstrated that the methodology is an applicable and powerful tool for blister studies of the PEM. The encouraging results from this work suggest future studies to validate fatigue, explore membrane electrode assembly (MEA), etc.

Future Work

Although significant strides have been made throughout this study, much work remains to be done before the bridge between ex-situ mechanical durability studies on PEM can be fully extended into in-situ fuel cell durability understanding. Following are some suggestions on future work to wrap up these efforts as well as potential extensions into other issues:

- The characterization of biaxial strength/lifetime properties has been significantly advanced by the refined stress analysis methods discussed herein. While the LVE Hencky shows some discrepancies from FEA and DIC methods, it provides computationally cheap, reasonable first-order approximations. Applications requiring the utmost precision should utilize finite element analysis methods.
- Although the DIC results provided encouraging insight into this study, further efforts to improve and standardize the procedure are needed. “Lightly misting with spray paint” is difficult to standardize from one researcher to another. Exploring methods such as airbrushing or printing could improve this. Similarly, the sphere fitting procedure remains somewhat of a black box and can use refinement (although investigations shown in the Appendix are efforts to further understand the procedure). A more robust method of fitting only the central region of the blister as well as exploring other potential candidates for fitting should be investigated.

- Fatigue testing should be analyzed with the DIC to validate the fatigue FEA histories. This would further strengthen the conclusions of this thesis.
- The DIC methodology could be extended to other materials, such as the membrane electrode assembly (MEA) which consists of PEM plus catalyst layer. Similarly, the DIC could be used at lower temperatures and smaller strains to measure the Poisson's ratio and biaxial modulus of the PEM.
- More data should be collected to further develop the residual strength based lifetime prediction model. A survey of interrupted constant pressure tests (CP test for part of the lifetime interrupted by a ramp to fail test) would provide the data necessary to determine an appropriate value for γ.
- Additional data for Gore-Select® Series 57 constant pressure and fatigue collected at different temperatures would provide further validation/invalidation of the lifetime prediction model. Since TTSP was found to work for quasi-static burst strength studies, this data and model extension would prove particularly interesting.
- The models should be further extended and evaluated based on more complex loading profiles. Cyclic fatigue with varying duty cycles, predictions based on uniaxial testing, RH cycling stress histories, etc. would all provide valuable insight into how robust or 1-dimensional the lifetime prediction models are.

References

[1] (Eia), E. I. A., 2008, "International Energy Outlook 2008," Department of Energy.
[2] Hegerl, G. C., Zweirs, F. W., Braconnot, P., Gillett, N. P., Luo, Y., Marengo Orsini, J. A., Nicholls, N., Penner, J. E., and Stott, P. A., 2007, Understanding and Attributing Climate Change, In Climate Change 2007: The Physical Science Basis. Contribution of Working Group I to the Fourth Assessment Report of the Intergovernmental Panel on Climate Change, Edited by.S. D. Solomon, et al. Cambridge University Press, Cambridge, United Kingdom and New York, NY, USA.
[3] Dresselhaus, M. S., and Thomas, I. L., 2001, "Alternative Energy Technologies," Nature, 414(6861), pp. 332-337.
[4] Energy, U. S. D. O., and Transportation, U. S. D. O., December 2006, "Hydrogen Posture Plan: An Integrated Research, Development and Demonstration Plan." U. S. DOE
[5] Huang, Z., and Zhang, X., 2006, "Well-to-Wheels Analysis of Hydrogen Based Fuel-Cell Vehicle Pathways in Shanghai," Energy, 31(4), pp. 471-489.
[6] Eg&G Technical Services, I., November 2002, "Fuel Cell Handbook (Seventh Edition)." U. S. DOE
[7] Nice, K., and Strickland, J., 2000, How Fuel Cells Work, http://auto.howstuffworks.com/fuel-cell2.htm
[8] Wu, J., Yuan, X. Z., Martin, J. J., Wang, H., Zhang, J., Shen, J., Wu, S., and Merida, W., 2008, "A Review of Pem Fuel Cell Durability: Degradation Mechanisms and Mitigation Strategies," Journal of Power Sources, 184(1), pp. 104-119.
[9] Kusoglu, A., Karlsson, A. M., Santare, M. H., Cleghorn, S., and Johnson, W. B., 2007, "Mechanical Behavior of Fuel Cell Membranes under Humidity Cycles and Effect of Swelling Anisotropy on the Fatigue Stresses," Journal of Power Sources, 170(2), pp. 345-358.
[10] Lai, Y.-H., Mittelsteadt, C. K., Gittleman, C. S., and Dillard, D. A., 2005, "Viscoelastic Stress Model and Mechanical Characterization of Perfluorosulfonic Acid (Pfsa) Polymer Electrolyte Membranes," ASME Conference Proceedings, 2005(37645), pp. 161-167.
[11] Solasi, R., Zou, Y., Huang, X., Reifsnider, K., and Condit, D., 2007, "On Mechanical Behavior and in-Plane Modeling of Constrained Pem Fuel Cell Membranes Subjected to Hydration and Temperature Cycles," Journal of Power Sources, 167(2), pp. 366-377.
[12] Tang, Y., Kusoglu, A., Karlsson, A. M., Santare, M. H., Cleghorn, S., and Johnson, W. B., 2008, "Mechanical Properties of a Reinforced Composite Polymer Electrolyte Membrane and Its Simulated Performance in Pem Fuel Cells," Journal of Power Sources, 175(2), pp. 817-825.
[13] Dillard, D. A., Li, Y., Grohs, J. R., Case, S. W., Ellis, M. W., Lai, Y.-H., Budinski, M., and Gittleman, C., *In Press*, "On the Use of Pressure-Loaded Blister Tests to Characterize the Strength and Durability of Proton Exchange Membranes," Journal of Fuel Cell Science and Technology.
[14] Li, Y., Dillard, D. A., Case, S. W., Ellis, M. W., Lai, Y.-H., Gittleman, C., and Miller, D. P., *In Review*, "Fatigue and Creep to Leak Tests of Proton Exchange Membranes Using Pressure-Loaded Blisters," Materials Science and Engineering: A.
[15] Energy, U. S. D. O., February 2004, "Hydrogen Posture Plan."
[16] Garbak, J., "Technology Validation 2007 D.O.E Hydrogen Program Merit Review," Washington DC.

[17] Hencky, H., 1915, "Über Den Spannungszustand in Kreisrunden Platten Mit Verschwindender Biegungssteiflgkeit," Zeitschrift fur Mathematik und Physik, 63(pp. 311-317.
[18] Hohlfelder, R. J., 1999, "Bulge and Blister Testing of Thin Films and Their Interfaces " Ph. D. Stanford University, Stanford.
[19] Arthur, V. T., 1956, "Stress Relaxation Studies of the Viscoelastic Properties of Polymers," AIP.
[20] Patankar, K., Dillard, D. A., Case, S. W., Ellis, M. W., Lai, Y.-H., Budinski, M., and Gittleman, C., In Preparation, "Hygrothermal Characterization of the Viscoelastic Properties of Gore Select 57 Proton Exchange Membrane " Mechanics of Time Dependent Materials.
[21] Haddad, Y. M., 1994, Viscoelasticity of Engineering Materials, Springer.
[22] Brinson, H. F., and Brinson, L. C., 2008, Polymer Engineering Science and Viscoelasticity an Introduction, Springer Science+Business Media, New York.
[23] Odegard, G., Gates, T., and Herring, H., 2005, "Characterization of Viscoelastic Properties of Polymeric Materials through Nanoindentation," Experimental Mechanics, 45(2), pp. 130-136.
[24] Sakai, M., and Shimizu, S., 2001, "Indentation Rheometry for Glass-Forming Materials," Journal of Non-Crystalline Solids, 282(2-3), pp. 236-247.
[25] Patankar, K., Dillard, D. A., Case, S. W., Ellis, M. W., Lai, Y.-H., Budinski, M., and Gittleman, C., In Preparation, "Characterizing Fracture Energy of Proton Exchange Membranes (Pem) Using a Knife Slit Test," Journal of Polymer Science.
[26] Cleghorn, S., Kolde, J., and Liu, W., 2003, "Catalyst Coated Composite Membranes", In Handbook of Fuel Cell - Fundamentals, Technology and Applications, Edited by.W. Vielstich, et al. John Wiley and Sons.
[27] Gittleman, C., Lai, Y.-H., and Miller, D., 2005, "Durability of Perfluorosulfonic Acid Membranes for Pem Fuel Cells," Proc. AIChE Annual Meeting Conference Proceedings, Cincinnati, OH.
[28] Ferry, J. D., 1980, Viscoelastic Properties of Polymers, Wiley, NY.
[29] Energy, U. S. D. O., 2002, National Hydrogen Energy Roadmap, http://www1.eere.energy.gov/hydrogenandfuelcells/pdfs/national_h2_roadmap.pdf
[30] Lai, Y.-H., and Dillard, D. A., 2009, Mechanical Durability Characterization and Modeling of Ionomeric Membranes, In Handbook of Fuel Cells Volume 5: Advances in Electrocatalysis Materials, Diagnostics and Durability, Edited by.A. W. Vielstich, et al. John Wiley & Sons, Ltd.
[31] Grohs, J. R., Li, Y., Dillard, D. A., Case, S. W., Ellis, M. W., Lai, Y.-H., Budinski, M., and Gittleman, C., *In Preparation*, "Evaluating the Time and Temperature Dependent Biaxial Strength of Gore-Select Series 57 Proton Exchange Membrane Using a Pressure Loaded Blister Test," Mechanics of Time Dependent Materials.
[32] Patankar, K., Dillard, D. A., Ellis, M. W., Case, S. W., Lai, Y.-H., Budinski, M., and Gittleman, C., 2007, "Characterizing Viscoelastic Properties of the Proton Exchange Membrane (Gore 57)," Proc. Society of Experimental Mechanics, Springfield, MA.
[33] Beer, F. P., Johnston, E. R. J., Dewolf, J. T., and Mazurek, D. F., 2009, Mechanics of Materials, McGraw-Hill, New York.
[34] Fedorov, A., Vellinga, W. P., and De Hosson, J. T. M., 2008, "Effects of Tensile and Compressive in-Plane Stress Fields on Adhesion in Laser Induced Delamination Experiments," Journal of Applied Physics, 103(10), pp. 103523-7.

[35] Jin, H., Lu, W. Y., and Korellis, J., 2008, "Micro-Scale Deformation Measurement Using the Digital Image Correlation Technique and Scanning Electron Microscope Imaging," The Journal of Strain Analysis for Engineering Design, 43(pp. 719-728.
[36] Willems, A., Lomov, S. V., Verpoest, I., and Vandepitte, D., 2008, "Optical Strain Fields in Shear and Tensile Testing of Textile Reinforcements," Composites Science and Technology, 68(3-4), pp. 807-819.
[37] Wipke, K., Sprik, S., Thomas, H., Welch, C., and Kurtz, J., "Controlled Hydrogen Fleet and Infrastructure Analysis," DOE Hydrogen Program: 2007 Annual Progress Report.
[38] Liu, W., Ruth, K., and Rusch, G., 2001, "Membrane Durability in Pem Fuel Cells," Journal of New Materials for Electrochemical Systems, 4(4), pp. 277-231.
[39] Tang, Y., Santare, M. H., and Karlsson, A. M., 2006, "Stresses in Proton Exchange Membranes Due to Hygro-Thermal Loading," Journal of Fuel Cell Science and Technology, 3(2), pp. 119-124.
[40] Grohs, J. R., Siuta, C. M., Mieritz, E., Case, S. W., Dillard, D. A., Ellis, M. W., Lai, Y.-H., Li, Y., and Gittleman, C., *In preparation*, "The Use of Digital Image Correlation and the Finite Element Method to Analyze Stresses in Pressure-Loaded Blister Tests of Proton Exchange Membranes " Mechanics of Time Dependent Materials.
[41] Guedes, R. M., 2007, "Durability of Polymer Matrix Composites: Viscoelastic Effect on Static and Fatigue Loading," Composites Science and Technology, 67(11-12), pp. 2574-2583.
[42] Loverich, J. S., Russell, B. E., Case, S. W., and Reifsnider, K. L., 2000, Life Prediction of Pps Composites Subjected to Cyclic Loading at Elevated Temperatures, In Time Dependent and Nonlinear Effects in Polymers and Composites, Edited by.R. A. Schapery, et al. American Society for Testing and Materials, West Conshonocken, PA.
[43] Miyano, Y., Nakada, M., Kudoh, H., and Muki, R., 2000, "Prediction of Tensile Fatigue Life for Unidirectional Cfrp," Journal of Composite Materials, 34(7), pp. 538-550.
[44] Miner, M., 1945, "Cumulative Damage in Fatigue," Journal of Applied Mechanics, pp. A159-A164.
[45] Sarkani, S., Michaelov, G., Kihl, D. P., and Bonanni, D. L., 2001, "Comparative Study of Nonlinear Damage Accumulation Models in Stochastic Fatigue of Frp Laminates," Journal of Structural Engineering, 127(3), pp. 314-322.
[46] Li, Y., Dillard, D. A., Case, S. W., Ellis, M. W., Lai, Y.-H., Gittleman, C., and Miller, D. P., 2009, "Fatigue and Creep to Leak Tests of Proton Exchange Membranes Using Pressure-Loaded Blisters," Materials Science and Engineering: A.

Appendix A:Tabulated Ramped Pressure Blister Data Summary Used in Chapter 2

A table of all ramped pressure blister data collected on Gore-Select® series 57 at 70℃,80℃, and 90℃ is presented in Table A.1. This data was used for the work in Chapter 2 and is presented below for future reference by the reader. It should be noted that the few samples performed on a reduced radius were exploratory tests to evaluate the effectiveness of a Teflon washer in the blister setup. Ultimately, the Teflon washer was not used, although the data is included with the modified 7.14375 mm value of the radius.

Table A.1: Ramped pressure blister data collected on Gore-Select® series 57 at 70℃, 80℃, and 90℃

Temperature	Radius (mm)	Pressure (kPa)	Time to Burst (s)	LVE Hencky Stress (MPa)
70℃	7.3	65.01	101	16.51
70℃	7.3	65.82	92	16.79
70℃	7.3	65.02	93	16.64
70℃	7.14375	67.42	169	15.82
70℃	7.3	49.77	293	12.33
70℃	7.3	54.58	226	13.50
70℃	7.3	76.25	36	20.06
70℃	7.14375	70.64	150	16.53
70℃	7.14375	75.45	103	17.94
70℃	7.3	73.85	36	19.64
70℃	7.3	73.04	36	19.50
70℃	7.3	85.08	5.8	24.72
70℃	7.3	82.67	9.2	23.59
70℃	7.3	84.28	8.8	23.96
70℃	7.3	80.27	20	21.82
70℃	7.3	74.65	25	20.40
80℃	7.3	51.35	134	10.70
80℃	7.3	44.15	186	9.30
80℃	7.3	41.72	253	8.63
80℃	7.3	44.15	223	9.10
80℃	7.3	43.33	213	9.04
80℃	7.3	45.73	191	9.49
80℃	7.3	53.79	92	11.50
80℃	7.3	55.40	68	12.11
80℃	7.3	56.19	60	12.38
80℃	7.3	59.41	56	12.94
80℃	7.3	61.81	53	13.36
80℃	7.3	59.38	51	13.06

80℃	7.3	61.81	31	14.15
80℃	7.3	59.38	30	13.83
80℃	7.3	64.21	31	14.52
80℃	7.3	51.35	133	10.71
80℃	7.3	49.74	106	10.75
80℃	7.3	48.16	97	10.63
80℃	7.3	64.21	14	15.85
80℃	7.3	65.82	14	16.11
80℃	7.3	69.03	13	16.76
80℃	7.3	73.04	8	18.23
80℃	7.3	71.44	5.2	18.63
80℃	7.3	70.63	5	18.55
80℃	7.3	74.65	5	19.25
90℃	7.3	64.21	6.6	11.77
90℃	7.3	61.81	7.4	11.32
90℃	7.3	61.00	10	10.81
90℃	7.3	56.99	12.2	10.09
90℃	7.3	56.19	16	9.70
90℃	7.3	51.39	29	8.59
90℃	7.3	56.99	31	9.14
90℃	7.3	50.56	31	8.44
90℃	7.3	51.39	32	8.50
90℃	7.3	42.54	42	7.28
90℃	7.3	43.34	43	7.35
90℃	7.3	40.13	65	6.67
90℃	7.3	43.36	77	6.89
90℃	7.3	42.54	78	6.79
90℃	7.3	40.14	78	6.53
90℃	7.3	39.35	127	6.11
90℃	7.3	32.10	139	5.28
90℃	7.3	36.13	142	5.71
90℃	7.3	32.10	182	5.14
90℃	7.3	31.30	183	5.06
90℃	7.3	30.50	185	4.96
90℃	7.3	33.71	197	5.27
90℃	7.3	30.50	258	4.81

Appendix B: Tabulated Ramped Pressure and Constant Pressure Lifetime Data Used for Painted/Unpainted Comparison in Chapter 3

A table of all ramped pressure blister data collected on both painted and unpainted Gore-Select® series 57 at 90℃ is presented in Table B.1. Table B.2 shows results of constant pressure blister testing on painted and unpainted Gore-Select® series 57 at 90℃. This data was used for validating the DIC methodology in Chapter 3 by showing that the effect of the spray paint on the mechanical lifetimes of the membrane is negligible.

Table B.1: Ramped pressure blister data collected on painted and unpainted Gore-Select® series 57 at 90℃

Time to Burst (s)	Applied stress rate (MPa)
Painted Samples	
8.6	3.04
9	3.04
9	3.04
9.1	3.04
10	3.04
10	3.04
21.4	1.04
22	0.65
22.8	0.65
23	1.04
23	1.04
24	1.04
26	1.04
27.4	0.86
28	0.65
30.4	0.86
38.7	1.04
40.4	0.65
42.8	0.65
44.4	0.65
68	0.41
73.2	0.41
73.5	0.41
131.5	0.22
133	0.22
133.7	0.22
140	0.22
141	0.22
141	0.22

Time to Burst (s)	Applied stress rate (MPa)
Unpainted Samples	
6.6	3.76
7.4	3.40
10	2.76
12.2	2.31
16	1.91
29	1.21
31	1.24
31	1.14
32	1.13
42	0.83
43	0.83
65	0.60
77	0.56
78	0.55
78	0.53
127	0.38
139	0.31
142	0.33
182	0.26
183	0.25
185	0.25
197	0.25
258	0.20

148.7	0.22
154	0.22
155	0.22
159	0.22
171	0.22
173.8	0.22
234.6	0.22
238	0.22
259	0.22

Table B.2: Constant pressure blister data collected on painted and unpainted Gore-Select® series 57 at 90℃

Time to failure (s)	Applied Stress (MPa)
Painted Samples	
544	2.90
460	2.90
480	2.90
358	3.64
470	3.63
222	3.66
226	3.66
150	3.70
578	3.63
32	5.59
8	6.44
10	6.30
43	5.50
37	5.54
35	5.56
17	5.93
16	5.97
36	5.55

Time to failure (s)	Applied Stress (MPa)
Unpainted Samples	
144092	1.96
107740	1.96
127861	1.96
101778	1.96
10184	2.37
12628	2.37
12024	2.37
16324	2.37
3346	2.75
3472	2.75
2945	2.75
2814	2.75
1397	3.11
1377	3.11
1717	3.11
1875	3.11
637	3.45
737	3.45
739	3.45
834	3.45
100	5.08
77	5.12
77	5.12
77	5.12

Appendix C: Mathematica Program Developed to Perform Linear Viscoelastic Hencky Stress Analysis for Ramped Pressure Testing

Shown here is a sample input/output from the Mathematica program used in calculating burst strength values for ramped pressure tests in Chapter 2. The data shown is for 70℃ but the same program structure was used for all temperatures and data of interest.

```
"The following is for 70 degrees C and Gore 57";
ClearAll["Global`*"]
"Define the appropriate material properties for Gore 57 at 70 degrees C";
e0 = 3;
e[1] = 2.019899;
τ[1] = .001;
e[2] = 2.019177;
τ[2] = .01;
e[3] = 2.948059;
τ[3] = .1;
e[4] = 50.78795;
τ[4] = 1;
e[5] = 67.19149;
τ[5] = 10;
e[6] = 48.76514;
τ[6] = 100;
e[7] = 24.59871;
τ[7] = 1000;
e[8] = 10.09611;
τ[8] = 10000;
e[9] = 4.684054;
τ[9] = 100000;
e[10] = 1.627818;
τ[10] = 1000000;

"Define the relaxation modulus E(t) as the prony series above";
erelax[t_] = e0 + ∑_{i=1}^{10} e[i] Exp[-t/τ[i]];
```

```
"Read in all of the experimental data so that a separate stress analysis can
   be performed on each experimental trial";
radii = {7.3, 7.3, 7.3, 7.14375, 7.3, 7.3, 7.3, 7.14375, 7.14375, 7.3, 7.3, 7.3, 7.3,
   7.3, 7.3, 7.3};
failpressures = {65.01, 65.82, 65.02, 67.42, 49.77, 54.58, 76.25, 70.64, 75.45,
   73.85, 73.04, 85.08, 82.67, 84.28, 80.27, 74.65};
failtimes = {101, 92, 93, 169, 293, 226, 36, 150, 103, 36, 36, 5.8, 9.2, 8.8, 20, 25};
ramprates = failpressures / failtimes;
howbig = Length[radii];
σ = Table[0, {i, howbig}];
"Cycle through each data point, calculating the stress at the time of blister
  failure - this is the burst strength reported."; For[j = 1, j ≤ howbig, j ++, (
  pressure[t_] := (ramprates[[j]] / 1000 * t);
  pprime23rds[t_] := D[(pressure[t]) ^ (2 / 3), t];
  b0 = 1.777;
  h = 0.018;
  σramp[t_] := b0 * (radii[[j]]) ^ (2 / 3) / 4 / h ^ (2 / 3) *
    NIntegrate[((erelax[(t - β)]) ^ (1 / 3) * pprime23rds[β]), {β, 0, t}];
  "This formula above is the convolution integral corresponding to the LVE
    Hencky solution"; σ[[j]] = σramp[(failtimes[[j]])];)]
σ
Export["sigma70.xls", σ]
```

```
{16.5087, 16.7909, 16.638, 15.8205, 12.3267, 13.4985, 20.0644, 16.5304,
 17.9375, 19.6411, 19.4973, 24.7214, 23.5885, 23.9628, 21.8199, 20.4032}
```

```
sigma70.xls
```

Appendix D: Mathematica Program Developed to Perform Linear Viscoelastic Hencky Stress Analysis for Constant Pressure and FatigueTesting

Shown here is a sample input/output from the Mathematica program used in calculating constant pressure and fatigue blister stress histories used in Chapter 3. The data is shown for 90℃ long-term testing of Gore-Select® Series 57 PEM.

```
"The following is for 90 degrees C and Gore 57";
ClearAll["Global`*"]
"Define the appropriate material properties for longterm testing of Gore 57 at 90 degrees C";
e0 = 8.5;
e[1] = 2.019899;
τ[1] = .001;
e[2] = 2.019177;
τ[2] = .01;
e[3] = 2.243603;
τ[3] = .1;
e[4] = 4.173175;
τ[4] = 1;
e[5] = 12.63559;
τ[5] = 10;
e[6] = 2.153934;
τ[6] = 100;

"Define the relaxation modulus E(t) as the prony series above";

erelax[t_] = e0 + Sum[e[i] Exp[-t / τ[i]], {i, 1, 6}];

"We can look at constant pressure by setting up for fatigue but using a period and pressurization
   time that keeps the program from cycling";
pressurelevel = 0.010;
period = 1 000 000;
pressurized = 1 000 000;
ncycles = 1;
pressure[t_] :=
 Sum[pressurelevel * HeavisideTheta[t - period * j] - pressurelevel * HeavisideTheta[t - pressurized - period * j],
  {j, 0, ncycles}]
pressurelevel = pressurelevel^(2 / 3);
Plot[pressure[t], {t, 0, ncycles * period}, AxesLabel → {"Time, sec", "Pressure^(2/3),Pa^(2/3)"}]
pprime[t_] := D[pressure[t], t];
```

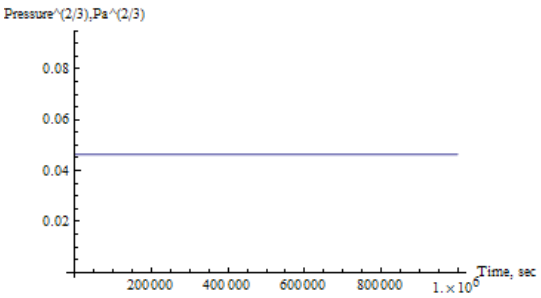


```
σcp[t_] := Sum[Integrate[((erelax[t - β]) / 1)^(1 / 3) * pprime[β], {β, -∞, t}] * HeavisideTheta[t - period * j] -
    Integrate[((erelax[t - β]) / 1)^(1 / 3) * pprime[β], {β, -∞, t}] * HeavisideTheta[t - pressurized - period * j], {j, 0, ncycles}]
```

```
"Now, lets examine the fatigue case.  The duty cycle we are modeling is 10-4 or 10 seconds pressuized
   and 4 seconds of relaxation time";
pressurelevel = 0.010;
period = 14;
pressurized = 10;
ncycles = 10;
pressure[t_] :=
 Sum[pressurelevel * HeavisideTheta[t - period * j] - pressurelevel * HeavisideTheta[t - pressurized - period * j],
  {j, 0, ncycles}]
pressurelevel = pressurelevel^(2 / 3);
Plot[pressure[t], {t, 0, ncycles * period}]
pprime[t_] := D[pressure[t], t];
```

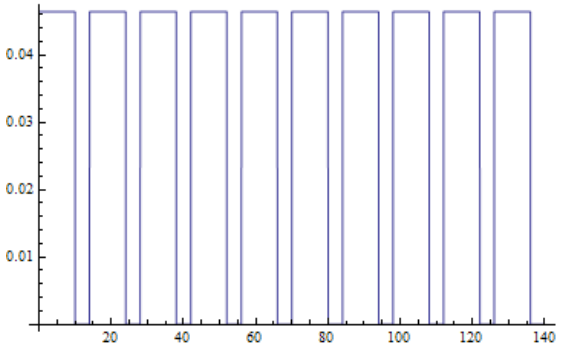

$$\sigma fat[t\_] := \text{Sum}\left[\text{Integrate}\left[\left(\frac{erelax[t-\beta]}{1}\right)^{(1/3)} * pprime[\beta], \{\beta, -\infty, t\}\right] * HeavisideTheta[t - period * j] - \text{Integrate}\left[\left(\frac{erelax[t-\beta]}{1}\right)^{(1/3)} * pprime[\beta], \{\beta, -\infty, t\}\right] * HeavisideTheta[t - pressurized - period * j], \{j, 0, ncycles\}\right]$$

Appendix E: Sphere Fitting Error Analysis Using LVE Hencky and FEA

In Chapter 3, all of the DIC stress analysis is performed using radius of curvature values obtained from a best-fit sphere algorithm within the ARAMIS software. This brief side study was used to analyze the potential error induced by the sphere fitting procedure by examining Hencky and FEA deformed geometries at a time of 1 second for a 14 kPa constant pressure case. The results are interesting but still somewhat puzzling and will be an area to focus on as the DIC work moves forward. Fitting a circular arc to the FEA nodal displacements shows significant dependence on the region fit. In going from fitting the entire shape to only fitting 1/8th of the shape, there is a 15% reduction in radius of curvature (which scales as a 15% reduction in stress.) This suggests that using the DIC to fit a sphere to the entire deformed shape would suggest that the obtained stress values would be significantly higher than actually experienced at the center. This would be due to an averaging effect from deformed areas with higher radius of curvature than at the center. In performing the same analysis on the Hencky deformed shape, the results showed less dependence on the region of fit of the deformed geometry. About 6% error was seen in comparing the entire region to a fit of 1/8th the radius. However, it is difficult to place significant confidence in these results since the stress values obtained from fitting the deformed shapes do not match up with the FEA stress values. Repeating the FEA and this analysis with threefold more elements (a 1200 SAX1 element model) resulted in no change in stress values or in fit radius of curvature values. It is postulated that the error in these values (on the order of 20-25%) is due to the dramatic sensitivity of curvature values to the sphere/circle fitting procedure when applied to discrete points. In the FEA, displacement values are obtained at the nodes while stress values are taken from the Gauss integration points and interpolation functions are used for intermodal displacements. Primitive shape interpolation as the cause of the error is also supported by the Hencky solution, which exhibits only 2% difference between Hencky stress values and stresses obtained from fit curvatures. Much remains to be learned from improving on this analysis. The programs used are shown below so that the work can be continued.

```
In[1]:= "The following is for 90 degrees C and Gore 57";
        ClearAll["Global`*"]
        a = 10.3;

In[4]:= "Import in the displacements of the nodes of the FEA model.  Note that this sample set of data is for t=1
          second of a 14 kPa constant pressure test";
        datawholeradius = Import["c:\documents and settings\jrgrohs\Desktop\FEA sphere fitting.csv"];

In[5]:= datawholeradius = SortBy[datawholeradius, First];

In[6]:= fitwholeradius = FindFit[datawholeradius, (x - x0)^2 + (y - y0)^2 - R^2, {x0, y0, R}, {x, y}]
        whole = ListPlot[Table[{datawholeradius[[i, 1]], datawholeradius[[i, 2]]}, {i, 1, 801}]];
        ysolwholeradius = Flatten[Solve[(x - x0)^2 + (y - y0)^2 == R^2, y] /. fitwholeradius][[2]]
        yvalueswholeradius[r_] := y /. ysolwholeradius /. x → r
        "Show[whole,Plot[{yvalueswholeradius[r]},{r,-a,a},PlotStyle→{{Red,Dashed,Thick},{Blue,Thick}},PlotRange→{{-a,a},{0,a}}]]"
         ;

Out[6]= {x0 → -2.71199 × 10^-16, y0 → -7.37174, R → 12.4424}

Out[8]= y → -7.37174 + √(154.813 - 5.42398 × 10^-16 x - x^2)
```

In[12]:=
```
dataonethirdradius = Table[datawholeradius[[i]], {i, 401 - 134, 401 + 134}];
```

In[13]:=
```
fitonethirdradius = FindFit[dataonethirdradius, (x - x0) ^2 + (y - y0) ^2 - R^2, {x0, y0, R}, {x, y}]
onethird = ListPlot[Table[{datawholeradius[[i, 1]], datawholeradius[[i, 2]]}, {i, 401 - 134, 401 + 134}]];
ysolonethirdradius = Flatten[Solve[(x - x0) ^2 + (y - y0) ^2 == R^2, y] /. fitonethirdradius][[2]]
yvaluesonethirdradius[r_] := y /. ysolonethirdradius /. x → r
```

Out[13]= $\{x0 \to 2.53166 \times 10^{-16},\ y0 \to -5.56337,\ R \to 10.7166\}$

Out[15]= $y \to -5.56337 + \sqrt{114.846 + 5.06332 \times 10^{-16}\, x - x^2}$

In[17]:=
```
"Show[whole,Plot[{yvaluesonethirdradius[r]},{r,-a,a},PlotStyle→{{Red,Dashed,Thick},{Blue,Thick}},PlotRange→{{-a,a},{0,a}}]]"
 ;
```

In[18]:=
```
datasmallerradius = Table[datawholeradius[[i]], {i, 401 - 50, 401 + 50}];
fitsmallerradius = FindFit[datasmallerradius, (x - x0) ^2 + (y - y0) ^2 - R^2, {x0, y0, R}, {x, y}]
ysolsmallerradius = Flatten[Solve[(x - x0) ^2 + (y - y0) ^2 == R^2, y] /. fitsmallerradius][[2]]
whole = ListPlot[Table[{datawholeradius[[i, 1]], datawholeradius[[i, 2]]}, {i, 1, 801}], PlotRange -> {{-a, a}, {0, 5.5}}];
yvaluessmallerradius[r_] := y /. ysolsmallerradius /. x → r
Show[whole, Plot[{yvaluessmallerradius[r], yvalueswholeradius[r], yvaluesonethirdradius[r]}, {r, -a, a},
  PlotStyle → {{Red, Dashed, Thick}, {Blue, Thick}, {Orange, Thick}, {Purple, Thick}}, PlotRange → {{-a, a}, {0, 5.5}}]]
```

Out[19]= $\{x0 \to 2.2911 \times 10^{-17},\ y0 \to -5.36816,\ R \to 10.5226\}$

Out[20]= $y \to -5.36816 + \sqrt{110.725 + 4.5822 \times 10^{-17}\, x - x^2}$

Out[23]=

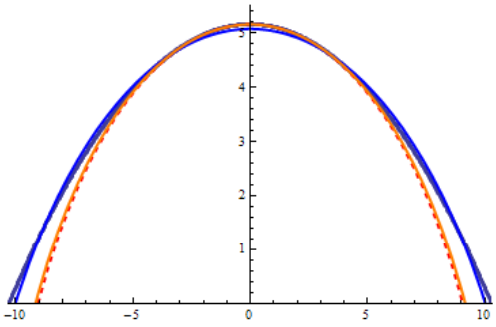

In[24]:=
```
p = 0.014;
h = 0.018;
ρwholeradius = R /. fitwholeradius[[3]];
ρonethirdradius = R /. fitonethirdradius[[3]];
ρsmallerradius = R /. fitsmallerradius[[3]];
```

In[29]:=
```
"Look at membrane force differences due to size of fit sphere";
p * ρwholeradius / 2
p * ρonethirdradius / 2
p * ρsmallerradius / 2
```

Out[30]= 0.0870966

Out[31]= 0.0750165

Out[32]= 0.0736583

In[33]:=
```
"Look at stress differences due to size of fit sphere";
p * ρwholeradius / 2 / h
p * ρonethirdradius / 2 / h
p * ρsmallerradius / 2 / h
"Percent difference in the calculated values"
(p * ρwholeradius / 2 / h - p * ρsmallerradius / 2 / h) / (p * ρwholeradius / 2 / h) * 100
```

Out[34]= 4.8387

Out[35]= 4.16758

Out[36]= 4.09213

Out[37]= Percent difference in the calculated values

Out[38]= 15.4292

In[55]:=
```
"The following is for 90 degrees C and Gore 57";
"Perform the same analysis using an assumed Hencky deflection for a 14 kPa constant pressure test for time=1 sec";
a = 10.3;
e = 23.6;
p = 14 / 1000;
h = 0.018;
σr[r_] :=
  1/4 ((a^2 e p^2)/h^2)^(1/3) (1.77687` - 0.31672962754871914` r^2/a^2 - 0.037638340440268696` r^4/a^4 - 0.0072681788828847255` r^6/a^6 -
    0.0016941981833686923` r^8/a^8 - 0.00043818629532514717` r^10/a^10 - 0.00012113171155462431` r^12/a^12 - 0.00003507580068403856` r^14/a^14 -
    0.00001051057156280 56` r^16/a^16 - 3.233511758023778`*^-6 r^18/a^18 - 1.0157437239970105`*^-6 r^20/a^20);
u[r_] :=
 a * (a * p / e / h)^(1/3) *
  (0.5799141625174081` (1 - r^2/a^2) + 0.05654899158931915` (1 - r^4/a^4) + 0.012253876546477091` (1 - r^6/a^6) +
    0.0032859983735814336` (1 - r^8/a^8) + 0.000978757461810705` (1 - r^10/a^10) + 0.00031056288129517595` (1 - r^12/a^12) +
    0.00010281124207276277` (1 - r^14/a^14) + 0.00003508788704154538` (1 - r^16/a^16) + 0.00001225289614197177` (1 - r^18/a^18) +
    4.356130198630079`*^-6 (1 - r^20/a^20))
```

In[63]:=
```
datawholeradiushencky = Table[{.1 * r, u[.1 * r], 0}, {r, -103, 103}];
```

In[64]:=
```
fitwholeradiushencky = FindFit[datawholeradiushencky, (x - x0)^2 + (y - y0)^2 - R^2, {x0, y0, R}, {x, y}]
```

Out[64]=
$$\{x0 \to -7.08679 \times 10^{-17},\ y0 \to -8.82095,\ R \to 13.4896\}$$

In[65]:=
```
ysolwholeradiushencky = Flatten[Solve[(x - x0)^2 + (y - y0)^2 == R^2, y] /. fitwholeradiushencky][[2]];
```

In[66]:=
```
yvalueswholeradiushencky[r_] := y /. ysolwholeradiushencky /. x → r
"Plot[{yvalueswholeradiushencky[r],u[r]},{r,-a,a},PlotStyle→{{Red,Dashed,Thick},{Blue,Thick}},PlotRange→{{-a,a},{0,a}}]";
```

In[68]:=
```
dataonethirdradiushencky = Table[{.03333 * r, u[.03333 * r], 0}, {r, -103, 103}];
```

In[69]:=
```
fitonethirdradiushencky = FindFit[dataonethirdradiushencky, (x - x0)^2 + (y - y0)^2 - R^2, {x0, y0, R}, {x, y}]
```

Out[69]=
$$\{x0 \to -1.47634 \times 10^{-16},\ y0 \to -8.11707,\ R \to 12.8118\}$$

In[70]:=
```
ysolonethirdradiushencky = Flatten[Solve[(x - x0)^2 + (y - y0)^2 == R^2, y] /. fitonethirdradiushencky][[2]];
```

In[71]:=
```
datasmallerradiushencky = Table[{1/80 * r, u[1/80 * r], 0}, {r, -103, 103}];
```

In[112]:=
```
fitsmallerradiushencky = FindFit[datasmallerradiushencky, (x - x0)^2 + (y - y0)^2 - R^2, {x0, y0, R}, {x, y}]
ysolsmallerradiushencky = Flatten[Solve[(x - x0)^2 + (y - y0)^2 == R^2, y] /. fitsmallerradiushencky][[2]];
yvaluessmallerradiushencky[r_] := y /. ysolsmallerradiushencky /. x → r
```

Out[112]=
$$\{x0 \to -2.75426 \times 10^{-17},\ y0 \to -8.04697,\ R \to 12.742\}$$

In[115]:=
```
ysolonethirdradiushencky = Flatten[Solve[(x - x0)^2 + (y - y0)^2 == R^2, y] /. fitonethirdradiushencky][[2]];
```

In[116]:=
```
yvaluesonethirdradiushencky[r_] := y /. ysolonethirdradiushencky /. x → r
Plot[{yvaluesonethirdradiushencky[r], yvaluessmallerradiushencky[r], u[r], yvalueswholeradiushencky[r]},
 {r, -a, a}, PlotStyle → {{Red, Dashed, Thick}, {Blue, Thick}, {Purple, Dashed, Thick}}, PlotRange → {{-a, a}, {0, 5}}]
```

Out[117]=

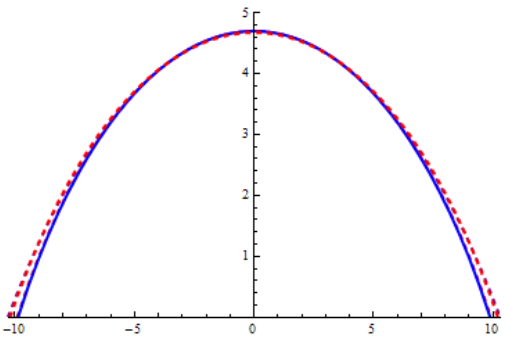

```
In[118]:= ρwholeradiushencky = R /. fitwholeradiushencky[[3]];
          ρonethirdradiushencky = R /. fitonethirdradiushencky[[3]];
          ρsmallerradiushencky = R /. fitsmallerradiushencky[[3]];

In[121]:= p * ρwholeradiushencky / 2 / h
          p * ρonethirdradiushencky / 2 / h
          p * ρsmallerradiushencky / 2 / h
          "percent error"
          (p * ρwholeradiushencky / 2 / h - p * ρsmallerradiushencky / 2 / h) / (p * ρsmallerradiushencky / 2 / h) * 100
          "Compare to Hencky stress at center and look at error induced"
          σr[0]
          "percent error between fit and hencky solution"
          (σr[0] - p * ρonethirdradiushencky / 2 / h) / σr[0] * 100

Out[121]= 5.24594

Out[122]= 4.98238

Out[123]= 4.95523

Out[124]= percent error

Out[125]= 5.86682

Out[126]= Compare to Hencky stress at center and look at error induced

Out[127]= 5.10146

Out[128]= percent error between fit and hencky solution

Out[129]= 2.33434
```

Appendix F: Sphere Fitting Error Analysis Using Full-Field DIC Displacement Data

Shown here is the Mathematica program developed to process an arbitrary set of (x coordinate, y coordinate, z displacement) data such as obtained from ARAMIS. The program imposes the axisymmetric nature of the data and finds the center based on some selected curve fit. Having found the center and this best fit curve, the curvature can be used to calculate the stress at the center of the blister and compared to the DIC sphere fitting routine. Although this will remain a work in progress/future work, this initial investigation suggests that the sphere fitting procedure could be providing slightly higher radius of curvature values than actually observed at the center of the blister. It is interesting to note that ARAMIS sphere fitting algorithms and this program show approximately 5% difference in stress values calculated when the entire region is selected. This difference gets smaller as the Mathematica program looks at smaller regions of data, even when compared to the ARAMIS sphere fit of all the data. To further confuse the phenomenon, selecting smaller regions of data within ARAMIS and re-processing appears to have no effect on the radius of curvature values from the fit. Although there still remain many questions and issues to sort out, the program below can be used and modified to help investigate the observed discrepancies.

It is noted that in the portion of the program which allows for an arbitrary fit on the full field of data, the curvature values obtained are highly sensitive to the type of fit used and the region used in fitting. Because of this sensitivity it is difficult to directly draw any conclusions in comparing the results to the sphere fits mentioned in the previous paragraph as well as in comparisons to FEA and Hencky shapes. This is still under investigation and likely will remain future work for those continuing the DIC efforts.

In[821]:=
```
ClearAll["Global`*"]
a = 10.3;
data = Import["c:\documents and settings\jrgrohs\desktop\14 kpa full field disp z.csv"];
xvalues = data[[All, 1]];
yvalues = data[[All, 2]];
zvalues = data[[All, 3]];
dataset = Table[{xvalues[[i]], yvalues[[i]], zvalues[[i]], 0}, {i, 1, Length[xvalues]}];
datasetnozero = Table[{xvalues[[i]], yvalues[[i]], zvalues[[i]]}, {i, 1, Length[xvalues]}];
onethirddataset = Table[{xvalues[[i]], yvalues[[i]], zvalues[[i]], 0},
   {i, 4 / 12 * Length[xvalues], 8 / 12 * Length[xvalues]}];
onesixthdataset = Table[{xvalues[[i]], yvalues[[i]], zvalues[[i]], 0},
   {i, Floor[5 / 12 * Length[xvalues]], Floor[7 / 12 * Length[xvalues]]}];
```

In[831]:=
```
fitwholeradius = FindFit[dataset, (x - x0) ^2 + (y - y0) ^2 + (z - z0) ^ (2) - R^2, {x0, y0, z0, R}, {x, y, z}]
fitonethirdradius = FindFit[onethirddataset, (x - x0) ^2 + (y - y0) ^2 + (z - z0) ^ (2) - R^2, {x0, y0, z0, R}, {x, y, z}]
fitonesixthradius = FindFit[onesixthdataset, (x - x0) ^2 + (y - y0) ^2 + (z - z0) ^ (2) - R^2, {x0, y0, z0, R}, {x, y, z}]
```

Out[831]= {x0 → 0.0888267, y0 → -1.41473, z0 → -14.1692, R → 18.0619}

Out[832]= {x0 → 0.109852, y0 → -1.42197, z0 → -13.7973, R → 17.6975}

Out[833]= {x0 → 0.1171, y0 → -1.41963, z0 → -13.8062, R → 17.7039}

In[834]:=
```
"DIC raw data fit with a sphere - stress value in MPa" 0.014 * 18.0619 / 2 / 0.018
"1/3 region - DIC raw data fit with a sphere - stress value in MPa"
0.014 * 17.6975 / 2 / 0.018
"Increasing small region - DIC raw data fit with a sphere - stress value in MPa"
0.014 * 17.7039 / 2 / 0.018
"Percent error between whole sphere and small region fits"
(0.014 * 18.0619 / 2 / 0.018 - 0.014 * 17.7039 / 2 / 0.018) / (0.014 * 17.7039 / 2 / 0.018) * 100
```

Out[834]= 7.02407 DIC raw data fit with a sphere - stress value in MPa

Out[835]= 1/3 region - DIC raw data fit with a sphere - stress value in MPa

Out[836]= 6.88236

Out[837]= Increasing small region - DIC raw data fit with a sphere - stress value in MPa

Out[838]= 6.88485

Out[839]= Percent error between whole sphere and small region fits

Out[840]= 2.02215

In[841]:=
```
"DIC raw data fit with a sphere - stress value in MPa"
0.014 * 18.0619 / 2 / 0.018
"ARAMIS sphere fit - stress value in MPa"
0.014 * 17.21 / 2 / 0.018
"Percent error between DIC measurement and sphere fit with raw data"
(0.014 * 18.0619 / 2 / 0.018 - 0.014 * 17.21 / 2 / 0.018) / (0.014 * 17.21 / 2 / 0.018) * 100
```

Out[841]= DIC raw data fit with a sphere - stress value in MPa

Out[842]= 7.02407

Out[843]= ARAMIS sphere fit - stress value in MPa

Out[844]= 6.69278

Out[845]= Percent error between DIC measurement and sphere fit with raw data

Out[846]= 4.95003

```
"This program will try out different potential 'centers' based on the axisymmetric nature of the
   blister.  When the correct center has been chose, all of the data will collapse on a blister
   height versus radius plot, and this will be the fit resulting in the least squared error.
   Different fit models can be used... in this case, a simple 3rd order polynomial is used.  Some
   sample output is shown but the full output was trimmed for simplicity";
sum = 20;
For[k = 0, k ≤ 3000, k++,
 (For[j = 0, j ≤ 3000, j++, (center = {1.5 - .001 * k, 1.5 - .001 * j};
    rvalues = Table[Sqrt[(xvalues[[i]] - center[[1]]) ^2 + (yvalues[[i]] - center[[2]]) ^2], {i, 1, Length[xvalues]}];
    polardata = Table[{rvalues[[i]], zvalues[[i]]}, {i, 1, Length[xvalues]}]; model = b * t^3 + c * t^2 + d * t + e;
    fit = FindFit[polardata, model, {b, c, d, e}, t];
    modelf = Function[{t}, Evaluate[model /. fit]];
    "Plot[modelf[t],{t,0,Sqrt[2]*a},PlotRange->{{0,2a},{0,2a}},Epilog→Map[Point,polardata]]";
    {tl, yl} = Transpose[polardata];
    residuals2 = (yl - Map[modelf, tl]) ^2;
    sumtrial = Total[residuals2]; If[sumtrial < sum, (Print[center]; Print[sum]; sum = sumtrial)])])]
```

```
{0.098, -1.399}
13.4847
{0.089, -1.399}
13.3319
{0.089, -1.4}
13.328
{0.074, -1.401}
13.2232
{0.074, -1.402}
13.2228
```

```
center = {0.074, -1.402};
rvalues = Table[Sqrt[(xvalues[[i]] - center[[1]]) ^2 + (yvalues[[i]] - center[[2]]) ^2], {i, 1, Length[xvalues]}];
"θvalues=Table[ArcTan[(yvalues[[i]]-center[[2]])/(xvalues[[i]]-center[[1]])],{i,1,numberofpoints}]";
polardata = Table[{rvalues[[i]], zvalues[[i]]}, {i, 1, Length[xvalues]}];
ListPlot[polardata, PlotRange → {{0, Sqrt[2] * a}, {0, Sqrt[2] * a}}]
"A collapsed plot here is expected when the center has been located";
```

Out[27]=

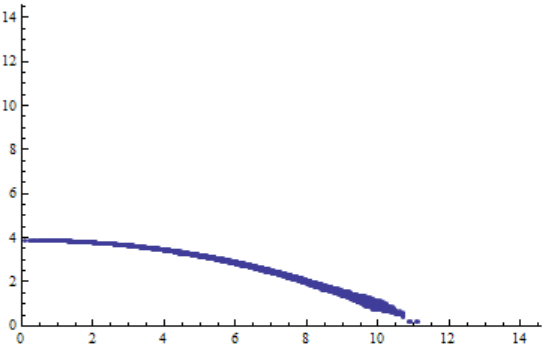


```
polardatafit = Table[{rvalues[[i]], zvalues[[i]], 0}, {i, 1, Length[xvalues]}];
model = b * t^3 + c * t^2 + d * t + u;
fit = FindFit[polardata, model, {b, c, d, u}, t];
"model=b*t;
   fit=FindFit[polardata,model,{b,c},t];";
modelf = Function[{t}, Evaluate[model /. fit]];
"Plot[modelf[t],{t,0,Sqrt[2]*a},PlotRange->{{1,5},{3.5,4.5}},Epilog→Map[Point,polardata]]";
{tl, yl} = Transpose[polardata];
residuals2 = (yl - Map[modelf, tl]) ^2;
sum = Total[residuals2]
"Plot[modelf[t],{t,0,Sqrt[2]*a},PlotRange->{{0,1},{3.5,4.5}},Epilog→Map[Point,polardata]]"
```

Appendix G: Mathematica Program to Develop Linear Damage Accumulation Based Lifetime Prediction Model from Constant Pressure Testing and Make Fatigue Predictions

Shown here is a sample input/output from the Mathematica program used in developing the linear damage accumulation lifetime prediction model of Chapter 4. The first part of the program uses constant pressure data to find the best fit (A,B) pair of lifetime prediction constants. The second part takes an input (A,B) and FEA fatigue stress histories to make fatigue lifetime predictions.

```
ClearAll["Global`*"]

"Read in experimental data used to calibrate/develop the model";
experimentaltimes = {144 092, 107 740, 127 861, 101 778, 10 184, 12 628, 12 024, 16 324, 3346, 3472, 2945, 2814, 1397,
   1377, 1717, 1815, 637, 737, 739, 834};
failedat = {0, 0, 0, 0, 0};
pressure = {6, 8, 10, 12, 14};

"Import the raw stress histories generated by ABAQUS";
data = Import["c:\documents and settings\jrgrohs\Desktop\Gore57 dry LDA CP FEA.csv"];

timehistories = {data[[All, 23]], data[[All, 19]], data[[All, 15]], data[[All, 11]], data[[All, 7]]};
stresshistories = {data[[All, 24]], data[[All, 20]], data[[All, 16]], data[[All, 12]], data[[All, 8]]};
cells = {65 000, 65 000, 65 000, 65 000, 65 000, 0};

"This program will find the best values A and B which minimized the logarithmic squared error between
   experimental and predicted failure times.  It functions on complete enumeration of A,B values within a
   specified range, and compares all of the error to find the best A,B pair";
errorgoal = .005;
working = 0;
For[o = 1, o < 401, o++, For[p = 1, p < 2, p++, For[k = 1, k < 991, k++, (c = Table[.1 * l, {l, 9900}];
    d = {5};
    "These are the A,B values... the range of interest is controlled by the iterating variables o,p, and k";
    guessingA = c[[k]] * 10^d[[p]];
    guessingB = Table[-4 - .01 * m, {m, 400}][[o]];
    inerror = 0.;
    failedat = {0, 0, 0, 0, 0};
    "This program runs from j=1-6 which is for the 6 different pressure levels of experimental data.  the
      failure criteria is for Linear Damage Accumululation.  Simple trapezoidal rule is used to numerically
      integrate through the time histories until failure";
    For[j = 1, j < 6, j++,
      (damage = 0; For[i = 2, i < cells[[j]], i++,
        (damage = damage + (timehistories[[j]][[i]] - timehistories[[j]][[i - 1]]) /
            ((guessingA * ((stresshistories[[j]][[i]])^guessingB + (stresshistories[[j]][[i - 1]])^guessingB)) / 2);
         If[damage ≥ 1, (failedat[[j]] = timehistories[[j]][[i - 1]]; i = 10 000;
           inerror = (inerror + (Log[failedat[[j]], 10] - Log[experimentaltimes[[(4 * j)]], 10])^2 +
              (Log[failedat[[j]], 10] - Log[experimentaltimes[[(4 * j - 1)]], 10])^2 +
              (Log[failedat[[j]], 10] - Log[experimentaltimes[[(4 * j - 2)]], 10])^2 +
              (Log[failedat[[j]], 10] - Log[experimentaltimes[[(4 * j - 3)]], 10])^2)); If[i == (cells[[j]] - 1), (inerror = 1)];];
         If[And[inerror > errorgoal, inerror ≠ 0], (j = 6;)])])]
     If[inerror < errorgoal, (Print[guessingA];
       Print[guessingB];
       Print[inerror]; Print[failedat]; errorgoal = inerror),
      (working = working + 1; If[Divisible[working, 1000], Print["working"]])])]]]
```

```
"Make fatigue predictions";
data = Import["c:\documents and settings\jrgrohs\Desktop\Gore 57 dry fatigue FEA.csv"];
timehistories = {data[[All, 27]], data[[All, 23]], data[[All, 19]], data[[All, 15]], data[[All, 11]], data[[All, 7]],
   data[[All, 3]]};
stresshistories = {data[[All, 28]], data[[All, 24]], data[[All, 20]], data[[All, 16]], data[[All, 12]], data[[All, 8]],
   data[[All, 4]]};
cells = {65535, 65535, 65535, 65535, 65535, 65535, 65535, 0};
guessA = 4.96 * 10^6;
guessB = -4.69;
failedat = {0, 0, 0, 0, 0, 0, 0};
For[j = 1, j < 8, j++,
 (damage = 0; For[i = 2, i < cells[[j]], i++,
   (damage = damage + (timehistories[[j]][[i]] - timehistories[[j]][[i - 1]]) /
       ((guessA * ((stresshistories[[j]][[i]])^guessB + (stresshistories[[j]][[i - 1]])^guessB)) / 2);
    If[damage ≥ 1, (failedat[[j]] = timehistories[[j]][[i - 1]]; i = 600000;)])])]
failedat
```

```
{62776.1, 32704.1, 14882.1, 11438.1, 7042.1, 3654.1, 2324.1}
```

Appendix H: Mathematica Program to Develop Residual Strength Based Lifetime Prediction Model from Constant Pressure Testing and Make Fatigue Predictions

Shown here is a sample input/output from the Mathematica program used in developing the residual strength based lifetime prediction model of Chapter 4. The first part of the program uses constant pressure data to find the best fit (A,B) pair of lifetime prediction constants. The second part takes an input (A,B) and FEA fatigue stress histories to make fatigue predictions.

```
ClearAll["Global`*"]
"Define material constants relevant to residual strength based model development";
sigult = 30;
gamma = 1;

"Read in experimental data used to calibrate/develop the model";
experimentaltimes = {144 092, 107 740, 127 861, 101 778, 10 184, 12 628, 12 024, 16 324, 3346, 3472, 2945, 2814, 1397, 1377,
   1717, 1815, 637, 737, 739, 834};
failedat = {0, 0, 0, 0, 0};
pressure = {6, 8, 10, 12, 14};

"Import the raw stress histories generated by ABAQUS";
data = Import["c:\documents and settings\jrgrohs\Desktop\Gore57 dry LDA CP FEA.csv"];

timehistories = {data[[All, 23]], data[[All, 19]], data[[All, 15]], data[[All, 11]], data[[All, 7]]};
stresshistories = {data[[All, 24]], data[[All, 20]], data[[All, 16]], data[[All, 12]], data[[All, 8]]};
cells = {65 000, 65 000, 65 000, 65 000, 65 000, 0};
howbig = cells[[1]];
residstren = Array[residstr, howbig];

"This program will find the best values A and B which minimized the logarithmic squared error between experimental
   and predicted failure times.  It functions on complete enumeration of A,B values within a specified range, and
   compares all of the error to find the best A,B pair";
errorgoal = .05;
working = 0;
For[o = 1, o < 41, o++, For[p = 1, p < 2, p++, For[k = 1, k < 991, k++, (c = Table[.1 * l, {l, 9900}];
    d = {5};
    "These are the A,B values... the range of interest is controlled by the iterating variables o,p, and k";
    guessingA = c[[k]] * 10^d[[p]];
    guessingB = Table[-4 - .01 * m, {m, 400}][[o]];
    inerror = 0.;
    failedat = {0, 0, 0, 0, 0};
    "This program runs from j=1-6 which is for the 6 different pressure levels of experimental data.  the failure
      criteria is for residual strength based modeling.  Simple trapezoidal rule is used to numerically integrate
      through the time histories until failure";
    For[j = 1, j < 6, j++,
      (residstr[1] = sigult;
       residstr[2] = sigult;
       For[i = 3, i < howbig, i++,
        (residstr[i] =
          (residstr[i - 1]^gamma - ((timehistories[[j]][[i]] - timehistories[[j]][[i - 1]]) / 2 *
               ((sigult^gamma - stresshistories[[j]][[i]]^gamma) / (guessingA * stresshistories[[j]][[i]]^guessingB) +
                 (sigult^gamma - stresshistories[[j]][[i - 1]]^gamma) / (guessingA * stresshistories[[j]][[i - 1]]^guessingB)))) ^ (1 / gamma);
         If[residstr[i - 1] ≤ stresshistories[[j]][[i - 1]], (failedat[[j]] = timehistories[[j]][[i - 1]]; i = howbig;
          inerror = (inerror + (Log[failedat[[j]], 10] - Log[experimentaltimes[[j]], 10]) ^2 +
               (Log[failedat[[j]], 10] - Log[experimentaltimes[[2 * j]], 10]) ^2 +
               (Log[failedat[[j]], 10] - Log[experimentaltimes[[3 * j]], 10]) ^2 +
               (Log[failedat[[j]], 10] - Log[experimentaltimes[[4 * j]], 10]) ^2) // N); If[i == (cells[[j]] - 1), (inerror = 1)];];
         If[inerror > errorgoal, (j = 6;)])])]
     If[And[inerror < errorgoal, inerror ≠ 0], (Print[guessingA];
       Print[guessingB];
       Print[inerror]; Print[failedat]; errorgoal = inerror), (working = working + 1; If[Divisible[working, 1000], Print["working"]])])]]]
```

```
"RS Fatigue Predictions"
guessA = 900 000;
guessB = -4.01;
σult = 30;
γ = 1;
failedat = {0, 0, 0, 0, 0};
For[j = 1, j < 6, j++, (
  residstr[1] = σult;
  For[i = 2, i < howbig, i++,
   (residstr[i] =
     (residstr[i - 1] ^γ - ((timehistories[[j]][[i]] - timehistories[[j]][[i - 1]]) / 2 *
          ((σult^γ - stresshistories[[j]][[i]]^γ) / (guessA * stresshistories[[j]][[i]] ^guessB) +
            (σult^γ - stresshistories[[j]][[i - 1]]^γ) / (guessA * stresshistories[[j]][[i - 1]] ^guessB)))) ^ (1 / γ);
    If[residstr[i - 1] ≤ stresshistories[[j]][[i - 1]], (failedat[[j]] = timehistories[[j]][[i - 1]]; i = howbig;)])];)]
failedat
residstr[2]
```

Appendix I: LDA model development and predictions for Nafion® NRE-211 at various times/temperatures

As mentioned in the future work section, combining the lifetime prediction model work with the TTSP findings of Chapter 2 could prove to be an interesting and insightful investigation. This initial investigation represents a brief look into using a LDA model with Nafion® NRE-211 experimental data and FEA stress histories. This development is not as robust or detailed as that presented in Chapter 4; however, it should be noted that this area is one which should be refined and given further attention in the future.

The LDA model was developed generally as in Chapter 4 for 90°C of NRE-211 but the FEA history inputs were simplified by fitting a power law. Again, for a more robust model, the procedures of Chapter 4 should be followed exactly for NRE-211. Alternately, this study could be performed on Gore-Select® Series 57 if constant pressure and fatigue data were collected for the material at different temperatures.

The model obtained values of A, B as (2.95×10^{9},-8.55). Shown in Figure I.1 is a summary plot of the model development as well as application of TTSP to shift the data. "Predictions" were made on the data at other temperatures by incorporating appropriate temperature shift factors into the general form of the LDA model.

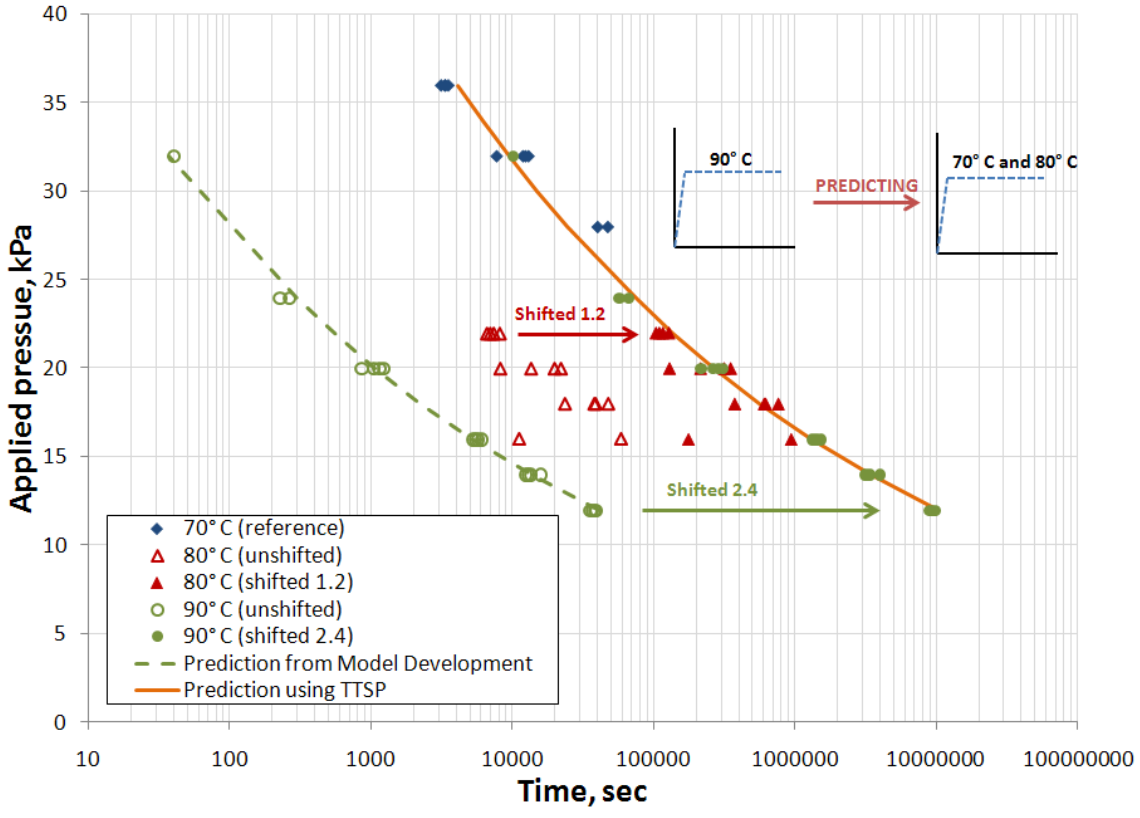

Figure I.1: LDA Model development and TTSP predictions on constant pressure testing of Nafion® NRE-211 at 70°C, 80°C, and 90°C

Using the model as developed above, some initial fatigue predictions were made. Unlike the constant pressure case, the fatigue histories cannot simply be multiplied by according shift factors since the experimental data was all collected at a 10-4 duty cycle. To make predictions, a FEA stress history is needed for each pressure level of interest as well as each temperature of interest. Because this is very computationally costly, only one 14 kPa curve was generated at 70° and 80° C. Future work, as suggested above, should focus either solely on one of the two membranes and robust, consistent development. This appendix is intended to spark interest in the topic, not provide solid conclusions one way or the other.